Flow, Turbulence and Combustion
https://doi.org/10.1007/s10494-021-00242-5

High-speed turbulent gas jets: an LES investigation of Mach and Reynolds number effects on the velocity decay and spreading rate

Francesco Bonelli[1] · **Annarita Viggiano**[2] · **Vinicio Magi**[2,3]

Received: 24 March 2020 / Accepted: 4 January 2021

Abstract
The aim of this work is the investigation of Mach and Reynolds numbers effects on the behaviour of turbulent gas jets in order to gain new insights into the fluid dynamic process of turbulent jet mixing and spreading. An in-house solver (Flow-Large Eddy and Direct Simulation, FLEDS) of the Favre-filtered Navier Stokes equations has been used. Compressibility has been analyzed by considering gas jets with Mach number equal to 0.8, 1.4, 2.0 and 2.6, and Re equal to 10,000. As concerns the influence of Re on gas jets, four cases have been investigated, i.e. Re = 2500, 5000, 10,000 and 20,000, with Mach number equal to 1.4. The results show that, in accordance with previous experimental and numerical studies, the potential core length increases with Mach number. As regards the velocity decay and the spreading rate downstream of the potential core, compressibility effects are not relevant except for the jet with Mach number of 2.6. The normalized turbulent kinetic energy along the centerline as a function of the normalized streamwise distance shows a similar peak at the end of the potential core for all jets, except for the case with Mach number of 2.6. By increasing Re, the length of the potential core decreases up to the same value for all Re higher than 10,000. In the region downstream of the potential core, the velocity decay decreases as Re number increases from 10,000 to 20,000, whereas, for lower values of Re, the influence is almost negligible.

Keywords Turbulent mass transfer · Gas jets · LES · Compressibility · Reynolds number · Velocity decay rate · Spreading rate

✉ Francesco Bonelli
francesco.bonelli@poliba.it

Annarita Viggiano
annarita.viggiano@unibas.it

Vinicio Magi
vinicio.magi@unibas.it; vmagi@sdsu.edu

[1] DMMM & CEMeC, Polytechnic University of Bari, 70125 Bari, Italy

[2] School of Engineering, University of Basilicata, 85100 Potenza, Italy

[3] Department of Mechanical Engineering, San Diego State University, San Diego, CA 92182, USA

Published online: 01 February 2021

1 Introduction

The physics of gas jets is a relevant topic for both fundamental fluid dynamics (Pope 2000; Wilcox 1994) and engineering applications (Hamzehloo and Aleiferis 2016). A round gas jet is formed when an axisymmetric flow, with a nearly uniform velocity, emerges into a medium at rest from a nozzle (Pope 2000). Along with wakes and mixing layers, free round jets are among the most important flows employed to investigate turbulence (Pope 2000; Wilcox 1994) from several points of view.

The flow characterization of steady incompressible round gas jets, in the absence of density/temperature ratios, heat release, phase transition and buoyancy, is well known and broadly studied (Boguslawski and Popiel 1979; Fellouah et al. 2009; Fellouah and Pollard 2009; Hussein et al. 1994; Panchapakesan and Lumley 1993; Weisgraber and Liepmann 1998; Wygnanski and Fiedler 1969; Xu and Antonia 2002). A comprehensive review can be found in the work of Ball et al. (2012). The structure of such "simple" jet is described by the mean streamwise velocity field, $\bar{u}_x(x, r)$, that is a function of the streamwise, x, and radial, r, coordinates. Usually, the mean streamwise centerline velocity, $\bar{u}_x(x, 0)$, and the mean half-width, $r_{1/2}$, (defined as the radial coordinate where the streamwise velocity is half of the velocity at the centerline, i.e. $\bar{u}_x(x, r_{1/2}) = \bar{u}_x(x, 0)/2$) are used as characteristic variables to verify self-similarity. Such a similarity consists of a collapse of the steady radial velocity profiles onto a single curve by using a proper scaling, i.e. $\bar{u}_x(x, r)/\bar{u}_x(x, 0) = f(\eta)$, where η is the similarity variable equal to $r/r_{1/2}$.

Thanks to the huge amount of experimental data and theoretical considerations, based on dimensional analysis and conservation laws (Chen and Rodi 1980), researchers were able to derive scaling laws useful to predict large scale jet characteristics such as the streamwise velocity decay rate and the spreading rate, i.e. the slope of $\bar{u}_x(0, 0)/\bar{u}_x(x, 0)$ and $r_{1/2}(x)$ profiles, respectively. Indeed, in the streamwise direction, downstream of the nozzle, three major regions can be identified: the near, intermediate and far fields. The near field is the region that includes the potential core, where the centerline velocity corresponds to the jet exit velocity, whereas the far field is the region where self-similarity and linear velocity decay hold, i.e. $\bar{u}_x(0, 0)/\bar{u}_x(x, 0)$ and $r_{1/2}(x)$ are straight lines. Between these two regions, there is an intermediate field, which is a developing flow region.

Although on one hand the features of incompressible jets are well consolidated, on the other hand the effects of density ratio (Amielh et al. 1996; Wang et al. 2008) and compressibility on jets still need further analysis. To fill this gap, in Bonelli et al. (2016) the authors have studied the behaviour of gas jets with large injection density ratios at high Reynolds number, whereas the present study aims to investigate the effects of compressibility at intermediate and high Mach numbers in the absence of shock and expansion waves, and the influence of a wide range of Re ($2500 < \mathrm{Re} < 20{,}000$) on the turbulence structure of such jets.

Compressibility identifies a flow regime where relative density variations become not negligible. For a steady isentropic quasi one-dimensional flow, relative velocity changes are related to relative density changes by means of the Mach number, M, by the following equation

$$d\rho/\rho = -M^2 du/u. \tag{1}$$

However, for flows without large density gradients, this is not sufficient to characterize the effects of compressibility on turbulence. Indeed, turbulence is affected by compressibility when density fluctuations, ρ', are important, or rather when the density fluctuations with respect to the mean value, $\rho'/\bar{\rho}$, are relevant (Morkovin's hypothesis) (Morkovin 1962).

Dealing with wall-bounded flows, such fluctuations are negligible up to a Mach number of about 5 (Wilcox 1994; Morkovin 1962), which is the low boundary of hypersonic flows and is far away from the incompressible limit of $M = 0.3$. Therefore, for wall-bounded flows, compressibility effects on turbulence are often negligible (Wilcox 1994, Cap. 5, p. 171). Instead, dealing with free shear flows, the relative density fluctuations become not negligible at relatively low Mach numbers; for some authors this happens around $M = 1$ (Wilcox 1994, Cap. 5, p. 172), for others around $M = 1.5$ (Bradshaw 1977).

The object of this paper has been dealt with starting from the early work of Morkovin (1962), followed by other research articles (Witze 1974; Papamoschou and Roshko 1988; Lau et al. 1979; Lau 1981; Maidi and Lesieur 2005; Wang and Andreopoulos 2010; Li et al. 2012; Bonelli et al. 2012, 2013b), review papers (Bradshaw 1977; Lele 1994; Gutmark et al. 1995) and text-books (Wilcox 1994). An important contribution has been given by the review work of Bradshaw (1977), whose main objective was "to substantiate, and qualify" previous statements concerning compressibility effects on turbulence and "to discuss the changes in turbulence structure that occur in hypersonic boundary layers" (free-stream Mach number greater than 5). Most of Bradshaw's paper focuses on boundary layers except for the last section that deals with shear flows. From his work, it can be concluded that, for shear flows, compressibility has a relevant influence on turbulence starting from about Mach number of 1.5. Moreover, most of the studies he mentioned concern with mixing layers and wakes, whereas the author points out that works on supersonic jets focused mainly on the investigation of shock and expansion waves. A significant aspect that Bradshaw highlighted is that, for both wakes and axisymmetric jets, velocity quickly decreases with the streamwise coordinate and the flow becomes incompressible after few nozzle or body diameters downstream.

Another important review was authored by Lele (1994), who described the effects of compressibility on turbulence and the introduction of dimensionless parameters used to characterize such effects and discussed homogeneous and simple inhomogeneous compressible flows to encourage development of turbulence modeling. Once again, in Lele's work it can be found a large amount of data on mixing layers and boundary layers but few references concerning turbulent gas jets. In particular, data regarding mixing layers, which show a reduction of the growth rate due to compressibility, are affected by a significant scatter (Lele 1994, Fig. 5).

An entire chapter devoted to compressibility effects on turbulence can be found in the book of Wilcox (1994), who provides a complete description of closure models that include compressibility effects.

Interesting experimental works on subsonic and supersonic free jets, without shock and expansion waves and with jet density and temperature equal to the ambient conditions, were carried out by Lau et al. (1979) and Lau (1981). Lau et al. (1979) studied the properties of three perfectly expanded isothermal gas jets, i.e. jets issuing at the same static temperature of the ambient, with exit Mach numbers equal to 0.28, 0.9 and 1.37. They found that, by increasing the Mach number, the potential core length, x_c, monotonically increases (Figs. 13 and 20 of Lau et al. 1979) and they suggested the following correlation:

$$\frac{x_c}{D} = 4.2 + 1.1M^2, \tag{2}$$

where D is the nozzle diameter.

As far as the velocity decay rate is concerned, Fig. 15 of Lau et al. (1979) does not show a significant influence of the Mach number on the jet except for the first few

diameters downstream of the potential core. Lau (1981) extended his previous work by considering, in addition to isothermal jets, also cold and heated jets with exit Mach numbers ranging from 0.28 to 1.67. As far as the potential core length is concerned, Fig. 13 of Lau (1981) shows that Eq. 1 is in agreement with measurements up to Mach 1.37, whereas for higher Mach numbers such a correlation underestimates experimental findings, as also pointed out by Lau (1981, p. 205).

As regards numerical works on the influence of compressibility on turbulent gas jets, a very recent work is performed by Bellan (2016) who employs a Large Eddy Simulation (LES) model to study perfectly expanded supersonic round jets, with jet temperature and density equal to ambient conditions, with Mach numbers equal to 1.4 and 2.1 and three Reynolds numbers (Re = 1500, 3700 and 7900). She found that, by increasing the Mach number, the potential core length increases, even if Fig. 5 of her paper shows that, with the highest Reynolds number, the velocity decay rate does not seem to be affected by compressibility. The same behavior was observed by LES findings of Maidi and Lesieur (2005) who studied two round gas jets at Mach number equal to 0.7 and 1.4. In fact, as Mach number increases, the potential core increases whereas the velocity decay rate seems not to be affected (see Fig. 8 of Maidi and Lesieur 2005).

An interesting work was presented by Witze (1974) who suggested an empirical law for the centerline velocity decay by using several experimental data. In addition to the aforementioned experimental and numerical works, other researchers dealt with the compressibility effects of free jets where shock and expansion waves occur and/or the jet to ambient temperature/density ratios differ from 1 (Zaman 1998, 1999; Gojon et al. 2019). Moreover, many works (DeBonis and Scott 2002; Boersma and Lele 1999; Buchta and Freund 2017; Freund 2019) have dealt with compressible jets in the context of noise reduction. For example an LES of a perfectly expanded compressible jet was performed by DeBonis and Scott (2002) with the aim of showing that CFD can provide useful data for the Lighthill's acoustic analogy. The literature about the latter subject is very wide and more details can be found in the review works of Tam (1995) and Jordan and Colonius (2013).

In this work, an LES methodology is used to investigate compressibility effects on gas jets. Four jets with different Mach numbers, i.e. 0.8, 1.4, 2.0 and 2.6, have been analyzed. Unlike to previous works and in order to focus only on compressibility effect from others, the four jets differ only for the exit Mach number while retain the same exit jet momentum and the same Reynolds number with no density/temperature ratios, i.e. the jet exit density, temperature and pressure corresponds to the ambient conditions. Furthermore, unlike other authors, a much wider computational domain has been selected so that our investigation is not limited to few diameters downstream of the potential core but such an investigation includes the analysis of the intermediate and far fields as well. Different turbulent jet structures have also been investigated by considering several Reynolds numbers, i.e. Re = 2500, 5000, 10,000 and 20,000, with Mach number equal to 1.4.

Computations have been performed by using an in-house solver, named FLEDS (Flow-Large Eddy and Direct Simulation), which provides a high-order numerical accuracy and has been extensively used in the past for several investigations on turbulent gas jets (Anders et al. 2007; Bonelli et al. 2013a, 2016).

Considering that subsonic and supersonic gas jets with relevant compressibility effects are important for practical applications, especially in the field of aerospace propulsion, e.g. scramjet engines, turbojet/turbofan, rockets, but also in the automotive sector, e.g. direct injection engines, this work can be helpful to improve the design process. Indeed, RANS approach used in most commercial codes needs turbulence closure models that employ empirical heuristic constants often requiring *ad hoc* corrections in order to take into

account some phenomena such as compressibility effects. In this context, LES provides physical insights useful to untangle some open questions; one of those regards compressibility effects of turbulent gas jets.

This work significantly enhances the very few works (Bellan 2016; Maidi and Lesieur 2005) on the effects of compressibility, by changing only the Mach number (keeping constant Re and momentum) and by using a larger physical domain ($90D \times 45D \times 45D$). Besides, with respect to Bellan (2016) and Maidi and Lesieur (2005) a wider range of Mach, starting from 0.8 up to 2.6, has been investigated. By combining different values of Mach and Re, seven different jets have been analysed, in order to accurately capture the trend of the results. Moreover, each term of the Favre-averaged turbulence kinetic energy equation has been computed, in an attempt to quantify their weights on the turbulent kinetic energy budget and to understand the physics underlying the effects of compressibility. To the best of authors' knowledge, this is the first time that all terms of this equation have been computed and discussed for such high Mach numbers.

The work is organized as follows: the governing equations and numerical models are summarized in Sect. 2; Sect. 3 deals with the computational setup; then, numerical results are given and discussed in Sect. 4; finally conclusions are summarized in Sect. 5.

2 Mathematical model

FLEDS solves the Favre-Filtered Navier–Stokes (FFNS) equations for a multicomponent mixture of non-reacting thermally perfect gases. In order to perform LES simulations, high fidelity time and space discretization schemes are used to provide high-order numerical accuracy in a wide range of frequency and wavenumbers. Specifically, space discretization is handled by a sixth-order compact scheme, which is derived from a generalization of the classical Padé schemes and has a spectral-like resolution in a wide range of wavenumbers (Lele 1992). In order to reduce the computational cost and retain high space resolution, the physical space is discretized by using a stretched grid, which is transformed in a cubic uniform grid into the computational domain.

The method of lines is used to separate time and space discretization, i.e. at first space fluxes are computed and then a system of ODEs is solved (Hirsch 2007) with respect to time. Time integration is performed by using a low-storage four-step/fourth-order explicit Runge–Kutta scheme (Gill 1951), which is well suited for problems where central differencing schemes are used to discretize convective terms and has very good properties in terms of accuracy, stability and computational cost (Hirsch 2007). In order to avoid wave reflections from boundaries, the Navier–Stokes Characteristic Boundary Conditions (NSCBC), given in Poinsot and Lele (1992) and extended to multicomponent flows by Abraham and Magi (1997), were used.

As far as the sub-grid scale (SGS) model is concerned, FLEDS can employ either the physical models of Smagorinsky (Pope 2004), both classical and dynamic, or the so called Artificial-Fluid Large Eddy Simulation (AFLES) model. Such a model has been initially proposed by Cook (2007) and extended to multi-dimensional generalized coordinate systems by Kawai and Lele (2008). In the present work, the latter approach is preferred since its stability properties are required when a non-dissipative scheme is applied to supersonic flows that involve large steep gradients of the fluid dynamic variables.

The code is written in Fortran 90 and is fully parallelized by using Message Passing Interface (MPI) libraries. Further details on mathematical models, computational approach

and code performance and validation can be found in Bonelli et al. (2016), Bonelli et al. (2013a), Anders et al. (2007), Sayeed et al. (2011), Anders (2006), Bonelli (2013).

3 The computational setup

Mach numbers considered in this work are typical of propulsive jets powering civilian and military aircraft (Brès et al. 2017; Morrison and McLaughlin 1980), whereas relatively low-Reynolds numbers have been chosen in order to highlight turbulence transition, moreover they are also used in experimental works in order to make measurements easier and to highlight coherent-structures (Morrison and McLaughlin 1980).

For all computations, the injected gas corresponds to that of the ambient with the same thermodynamic conditions, i.e. pressure, density and temperature. Compressibility effects have been studied by considering four jets at Mach number equal to 0.8, 1.4, 2.0 and 2.6, respectively. In order to focus mainly on compressibility effects, all four jets have the same exit jet momentum and Reynolds number. Mach number has been changed by varying the exit gas temperature, i.e. the speed of sound. In other words, the gas jets have different exit temperature and pressure, but the same exit density. Furthermore, the streamwise velocity, the jet diameter and gas viscosity are kept the same for all computations.

In order to analyse the influence of turbulence on gas jets, the case with Mach number equal to 1.4 has been chosen and three additional gas jets with different Reynolds numbers have been considered, i.e., 2500, 5000 and 20,000. The Reynolds numbers have been selected by changing the molecular gas viscosity. In order to preserve the same Prandtl number (Pr), conductivity (κ) was varied accordingly.

The computational domain has an extension of $90D \times 45D \times 45D$ in the streamwise and spanwise directions, respectively. It was discretized by using a stretched Cartesian grid which includes approximately 103 million grid points, specifically $841 \times 351 \times 351$ along the three coordinate directions, respectively. The grid spacing varies from $0.039D$ to $0.165D$ and from $0.0343D$ to $0.409D$ in the streamwise and spanwise directions, respectively. A representation of the normalized computational domain along with the computational grid, drawn every ten grid points, is shown in Fig. 1.

A subsonic/supersonic inflow is selected at the inlet boundary where the following hyperbolic tangent profile is used to set the streamwise inlet velocity along the radial direction (r):

$$u(r) = \left(\frac{u_e + u_a}{2}\right) + \left(\frac{u_e - u_a}{2}\right) \tanh\left(\frac{r_0 - r}{2\delta_\theta}\right), \tag{3}$$

where u_e is the injected centerline velocity and u_a is a negligible coflow velocity. The ratio between momentum thickness and nozzle radius δ_θ / r_0 is set equal to 0.01 (Zaman 1985; Bogey et al. 2003; Bonelli et al. 2016). All other boundaries are subsonic non-reflecting (Poinsot and Lele 1992). Moreover, a random perturbation (vortex ring) has been applied at $0.4D$ downstream of the nozzle exit in order to induce turbulence transition (Bogey et al. 2003; Anders et al. 2007).

In what follows, results will be presented in terms of both instantaneous and Reynolds averaged ($< \cdot >$) quantities. In order to get Reynolds-averaged radial profiles of all the quantities, data have also been azimuthally averaged over roughly 1.0° angle increments. Despite the computations were performed by using a Cartesian coordinate system, a cylindrical coordinate

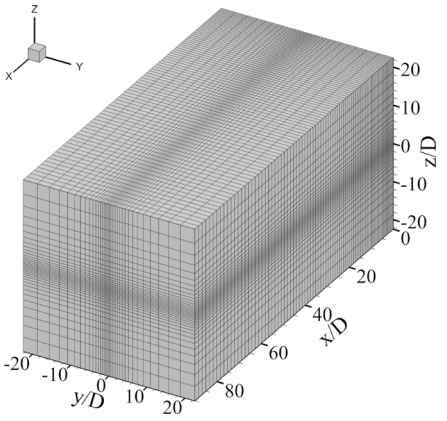

(a) 3D

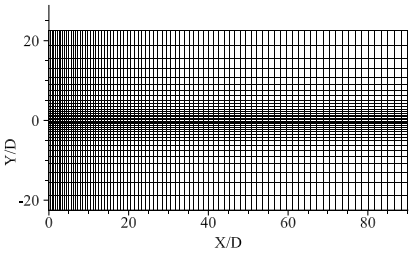

(b) x-y

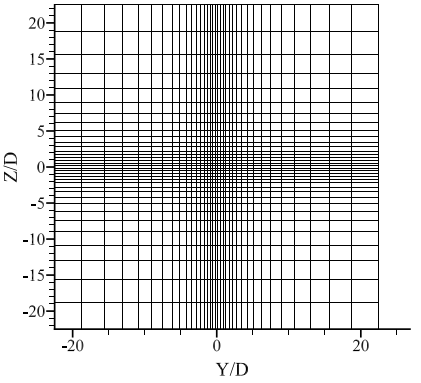

(c) y-z

Fig. 1 Computational domain and grid, drawn every ten grid points

system is also introduced due to the axisymmetry configuration of all test-cases. Hence, x and r refer to the streamwise and radial directions, respectively.

In order to study the jet turbulence characteristics, Favre averaging has been considered. Fluctuation of the i-th velocity component u_i is defined as:

$$u_i'' = u_i - \tilde{\bar{u}}_i, \tag{4}$$

where $\tilde{\bar{u}}_i$ is the Favre averaged velocity

$$\tilde{\bar{u}}_i = \frac{<\rho u_i>}{<\rho>}. \tag{5}$$

The instantaneous value of the Turbulent Kinetic Energy (TKE) is:

$$\mathrm{TKE} = \frac{1}{2}(u_x'' u_x'' + u_y'' u_y'' + u_z'' u_z''), \tag{6}$$

whereas Favre averaging has been used to compute its mean value:

$$\widetilde{\overline{\mathrm{TKE}}} = \frac{1}{2}\frac{<\rho u_x'' u_x''> + <\rho u_y'' u_y''> + <\rho u_z'' u_z''>}{<\rho>}. \tag{7}$$

4 Results

As a preliminary step, a space and time resolution study has been carried out by analysing the computed deterministic Power Spectrum Density (PSD) of all cases. Specifically, the averaging approach suggested by Welch (1967) has been employed to evaluate the PSDs. Figures 2 and 3 provide the PSDs, evaluated as TKE signals normalized by the squared jet exit velocity (TKE/u_e^2), for all test-cases with different Mach and Reynolds number, respectively. Besides, in the figures the signals computed with respect to both time and space are also given.

As far as the time signal is concerned, a location (along the centerline) is chosen for all jets to be enough downstream of the potential core, such that the turbulence spectrum is fully developed, homogeneous and isotropic. Moreover, such a location is chosen in a way that for all jets the normalized $\widetilde{\overline{\mathrm{TKE}}}$ is taken equal to 0.0065, which corresponds to $x/D = 17.5$, 18.9, 22.2 and 33.6 for Mach numbers equal to 0.8, 1.4, 2.0 and 2.6 respectively. For each jet about 800 time-samples, with a sampling period of 0.01 ms, are used, to achieve a very high value of Strouhal number, defined as $St = fD/u_x(0,0)$ with f, sampling frequency, equal to 4.48 and Nyquist limit that corresponds to $St = 2.24$. PSDs are given as a function of St at the top of both Figs. 2 and 3.

As far as space spectra are concerned, a straight line along the centerline is considered, which extends from a location where the normalized $\widetilde{\overline{\mathrm{TKE}}}$ is equal to 0.01 ($x/D = 15.2$, 16.0, 20.2 and 30.2 for Mach numbers equal to 0.8, 1.4, 2.0 and 2.6, respectively), which is sufficiently downstream of the potential core (where turbulence is fully developed), up to the end of the computational domain. PSDs are given as a function of wave number, k, at the bottom of Figs. 2 and 3 .

Figure 2 shows the PSDs for different Mach numbers, whereas Fig. 3 shows the PSDs for different Reynolds numbers. No appreciable differences are detected among the jets. All figures show a fully broadband spectrum, with the well known $-5/3$ Kolmogorov power law in the inertial range (Pope 2000), and the -7 power law in the dissipation range (Heisenberg 1948). This assesses the proper time and space resolutions which are used in this work.

Figures 4 and 5 show the instantaneous contour plots of the dimensionless vorticity ($\omega D/u_e$) at different Mach and Reynolds numbers, respectively, on a middle transverse plane. The figures show a high vorticity value along the edge of the potential core.

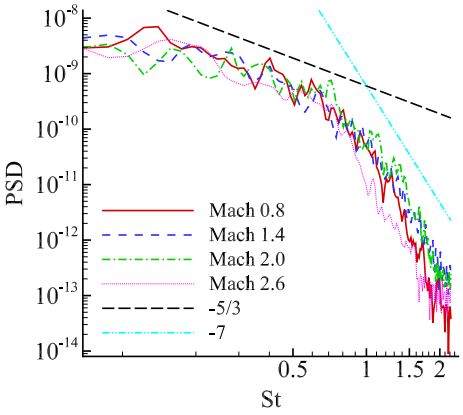

(a) PSD vs St

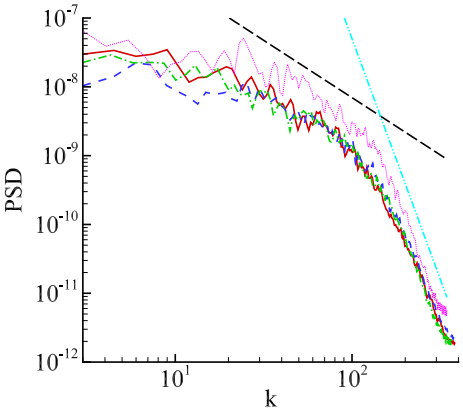

(b) PSD vs k

Fig. 2 Power spectrum density of the normalized TKE (TKE/u_e^2) for different Mach numbers: **a** PSD vs Strouhal number; **b** PSD vs wave number (k)

As the Mach number increases, the vorticity intensity decreases along the edge of the potential core, thus causing an increase of the core length as shown in Fig. 4. For the gas jet with Mach equal to 0.8, the vorticity at the end of the potential core is higher with respect to the other cases (see Fig. 4b). Consequently Kelvin-Helmholtz instabilities are more evident and finer fluid dynamics structures are generated. Transition to turbulence is less efficient by increasing the Mach number, thus generating a longer potential core and larger structures just downstream of the core. This finding is confirmed by similar results shown in the work of Bellan (2016, Figs. 3 and 4). On the other hand by an increase of the Reynolds number, the potential core length decreases and smaller scales are generated (see also Bellan (2016, Figs. 3 and 4). This is because, at smaller Re, viscosity contribution prevails on the inertial one and the energy transfer to smaller scales does not have enough time to occur since turbulent kinetic energy has already been dissipated into heat.

Figures 6 and 7 show the radial profile of the normalized mean streamwise velocity as a function of $r/r_{1/2}$, where $r_{1/2}$ is the jet mean half-width, at several streamwise locations in the fully developed turbulent region for all Mach and Reynolds numbers, respectively. All

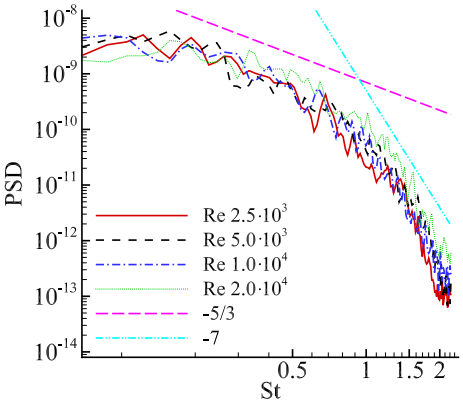

(a) PSD vs St

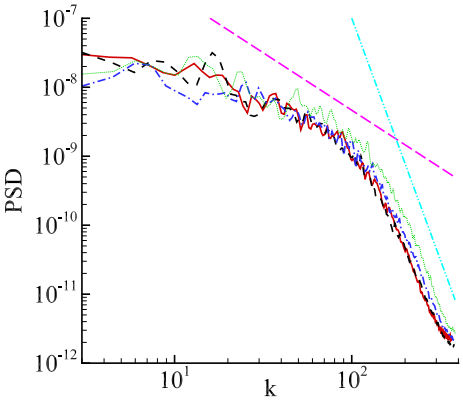

(b) PSD vs k

Fig. 3 Power spectrum density of the normalized TKE (TKE/u_e^2) for different Reynolds numbers: **a** PSD vs Strouhal number; **b** PSD vs wave number (k)

profiles collapse fairly well onto a single theoretical profile given by the following expression (Sautet and Stepowski 1995):

$$\frac{\bar{u}_x(x,r)}{\bar{u}_x(x,0)} = \exp\left[-\left(\frac{r}{r_{1/2}}\right)^2 \ln 2\right], \tag{8}$$

thus showing that the self-similarity is recovered also when compressibility effects are taken into account.

Figure 8a shows the inverse normalized centerline streamwise velocity as a function of the normalized streamwise distance for different Mach numbers and Re equal to 10,000. The numerical results are given along with those obtained by Bellan (2016) with Re equal to 7900 and Mach equal to 1.4 and 2.1. A good agreement with Bellan (2016) has been found although our jet conditions differ from Bellan. As already shown in Fig. 4, the potential core length (x_c) increases by increasing the Mach number. This is in agreement with the results of Bellan (2016).

A slight difference in the potential core length has been observed for low Mach numbers. Specifically, for gas jets with Mach number equal to 0.8 and 1.4, the computed potential

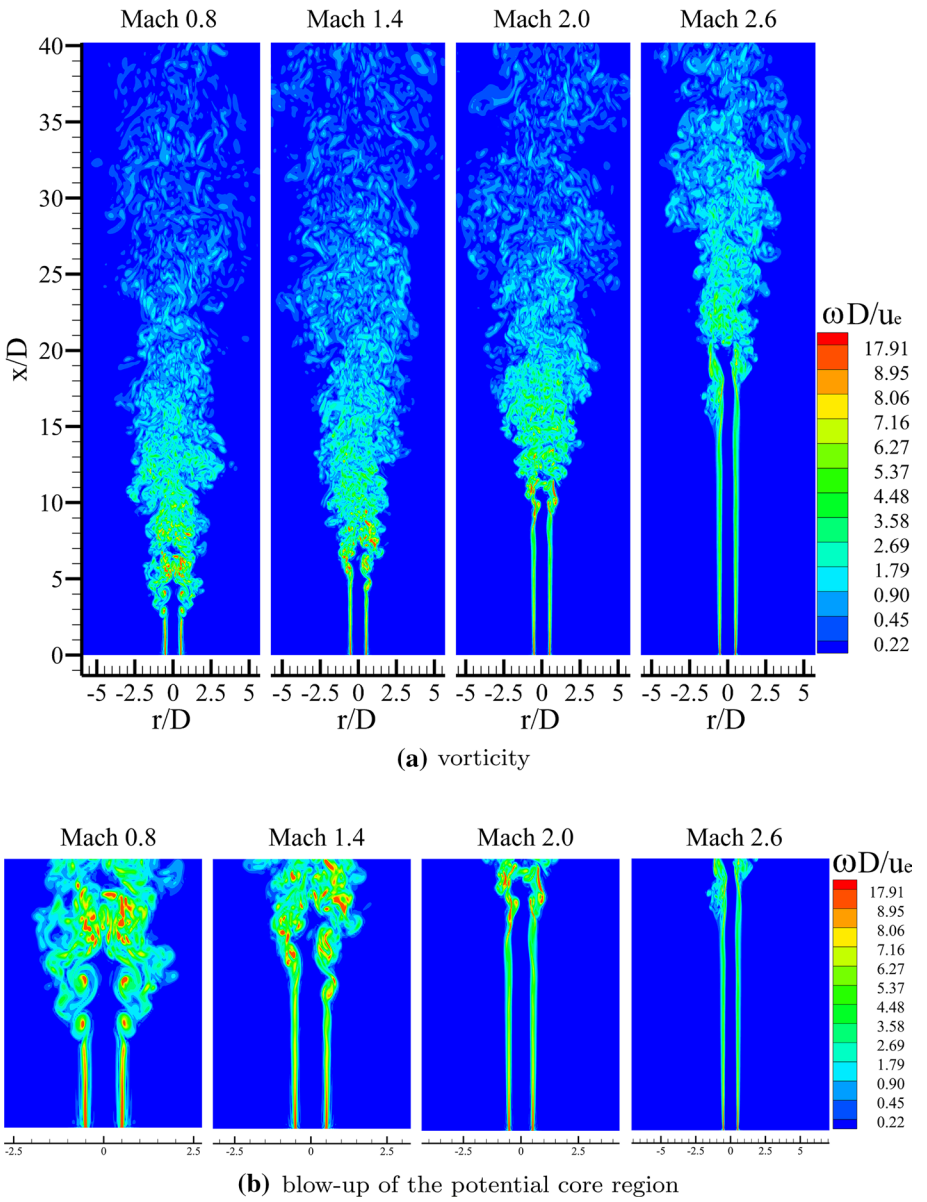

Fig. 4 Dimensionless vorticity ($\omega D/u_e$) contour plots for different Mach numbers

core length is in good agreement with the correlation proposed by Lau et al. (1979) (Eq. 1) and based on experimental measurements. Based on the definition of the streamwise distance x_c (Bogey and Bailly 2006), which is the streamwise distance where the centerline velocity is 95% of the injection velocity, the simulations with Mach equal to 0.8 and 1.4 provide x_c equal to 5.05 and 6.51, respectively. For higher Mach numbers, i.e. 2.0 and 2.6, the agreement is only qualitative, since the largest Mach number used in the experiments

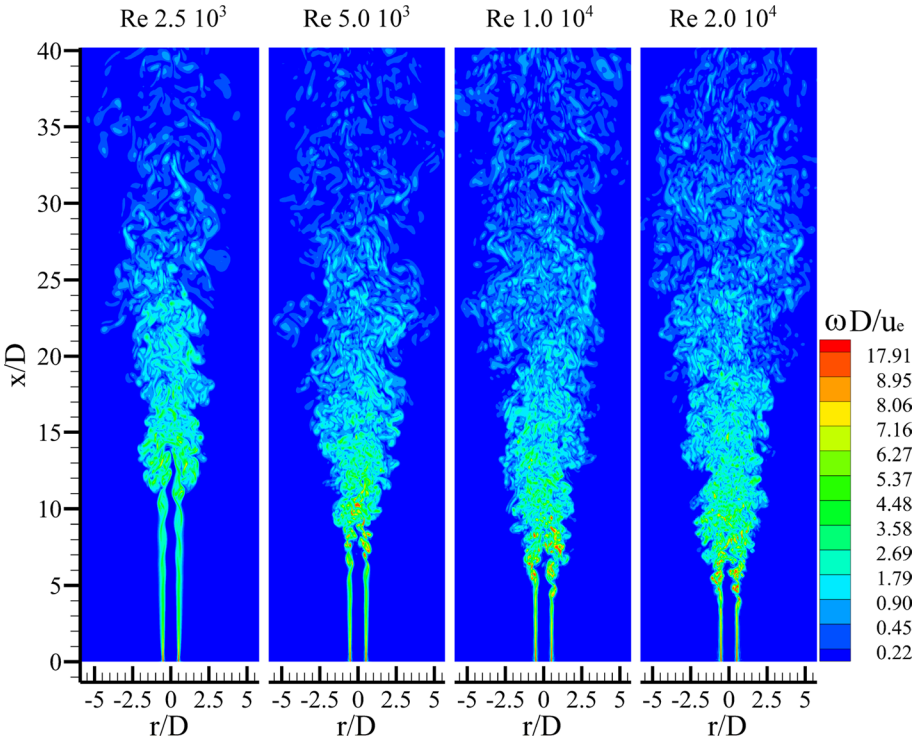

Fig. 5 Dimensionless vorticity ($\omega D/u_e$) contour plots for different Reynolds numbers

of Lau et al. (1979) is 1.37. Moreover, as already pointed out, Lau (1981) noticed, in his subsequent work, that his empirical correlation predicted smaller x_c than the measured one, for Mach numbers larger than 1.37 (see Fig. 13 of Lau (1981)). As far as the velocity decay downstream of the potential core is concerned, the influence of Mach numbers seems to be not so relevant. Indeed, in the region where steady conditions are achieved, the gas jet at Mach 2.6 shows a slightly lower decay. This is more clear from Fig. 9a, where the profiles are shifted along the x-axis by the potential core length. Figure 8b shows the normalized half-width as a function of the normalized streamwise distance, whereas Fig. 9b shows the same profile but shifted by the potential core length. Such figures confirm that a longer potential core length is recovered with higher Mach number jets, whereas compressibility effects downstream of the potential core are negligible even for the case with Mach equal to 2.6. This is because turbulence statistics, that will be shown in the following, are different in the region up to the potential core, but have similar magnitudes and trends in the fully developed flow region (see Fig. 12b).

Figure 10a shows the inverse normalized centerline streamwise velocity for different Reynolds numbers and Mach number equal to 1.4. By increasing Re, the potential core becomes shorter until it asymptotically reaches a constant value for Reynolds numbers higher than 10,000. This trend is in agreement with the outcomes of Bellan (2016), where the potential core length is longer for the jet with Re equal to 1500 with respect to the jets with Re equal to 3700 and 7900. Such a trend is much more evident in Bellan (2016) for the gas jet with Mach equal to 2.1 with respect to the jet with Mach equal to 1.4. The same

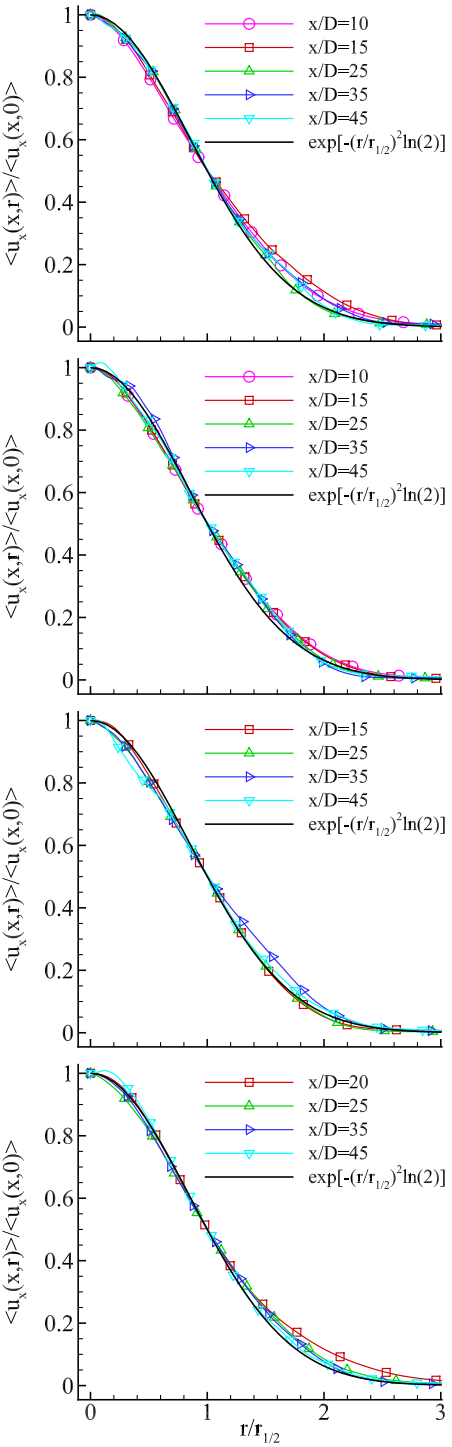

Fig. 6 Mean streamwise velocity radial profiles in similarity coordinates. From top to bottom: mach number equal to 0.8, 1.4, 2.0, 2.6

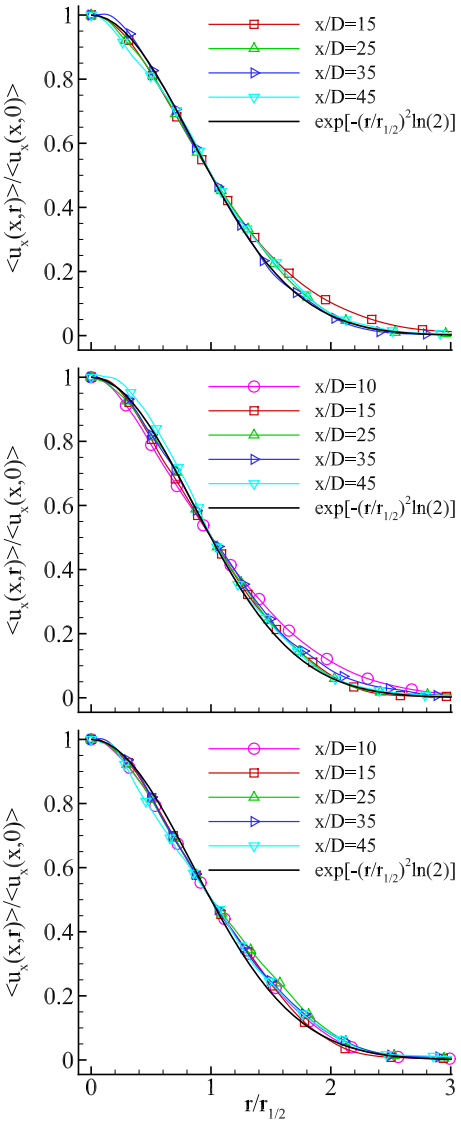

Fig. 7 Mean streamwise velocity radial profiles in similarity coordinates. From top to bottom: Reynolds number equal to 2.5×10^3, 5.0×10^3, 2.0×10^4

trend is also found in Bogey and Bailly (2006), where Reynolds number has been changed by varying only the jet diameter. Therefore, a change in the injected gas momentum occurs. Furthermore, a subsonic condition with Mach equal to 0.9 has been considered. In Bogey and Bailly (2006), the potential core length decreases by increasing the Reynolds number from 1700 to 10,000, whereas such a length is practically the same, within a 5% difference, for Re equal to 10,000 and 400,000. As regards the inverse normalized centerline streamwise velocity decay rate, our simulations show that the larger Re seems not to affect the jet decay rate downstream of the potential core up to Re 10,000. Conversely, from Re 10,000 to 20,000, the gas velocity decays slower. A decrease of the velocity decay rate with increasing Reynolds numbers has already been observed by Bogey and Bailly (2006), where the Reynolds number affects the velocity decay also for lower values of Re,

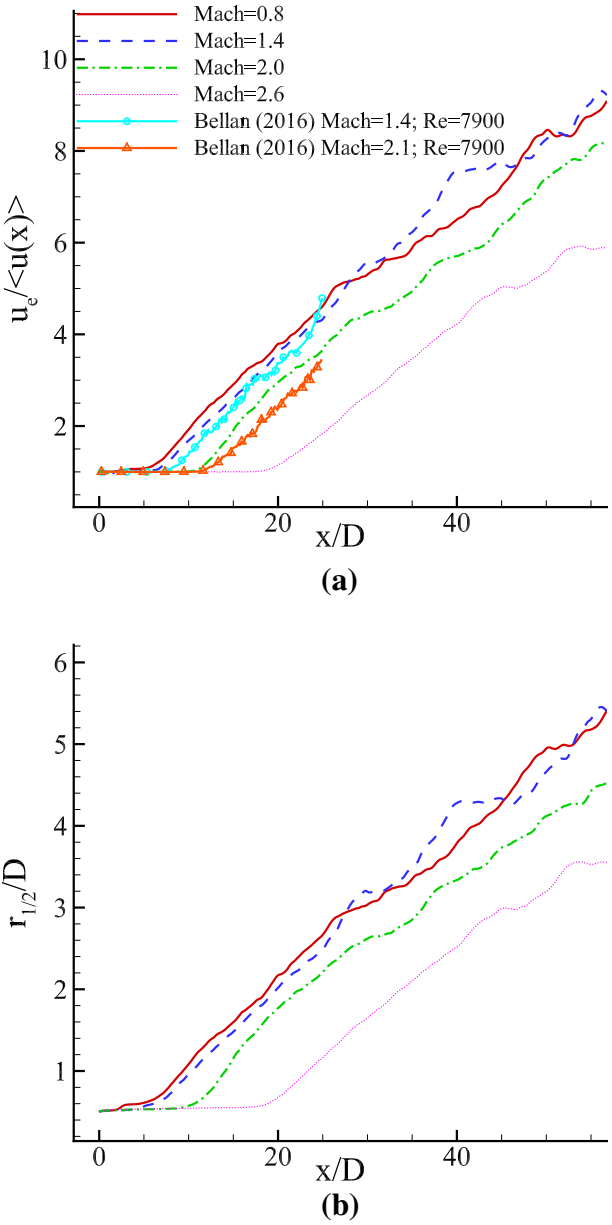

Fig. 8 **a** Inverse normalized centerline mean streamwise velocity and **b** normalized mean half-width vs normalized streamwise distance for different Mach numbers

and is consistent with findings of Freund (2001). The smaller decay rate for Re 20,000 is also confirmed by the spreading rate profiles (see Fig. 10b). Indeed, similar to the velocity decay rate, Re seems not to affect the spreading rate downstream of the potential core up to Re 10,000, whereas from Re 10,000 to 20,000 the spreading rate decreases. A plausible explanation is that, at Re equal to 20,000, a fully turbulent condition is reached, and TKE,

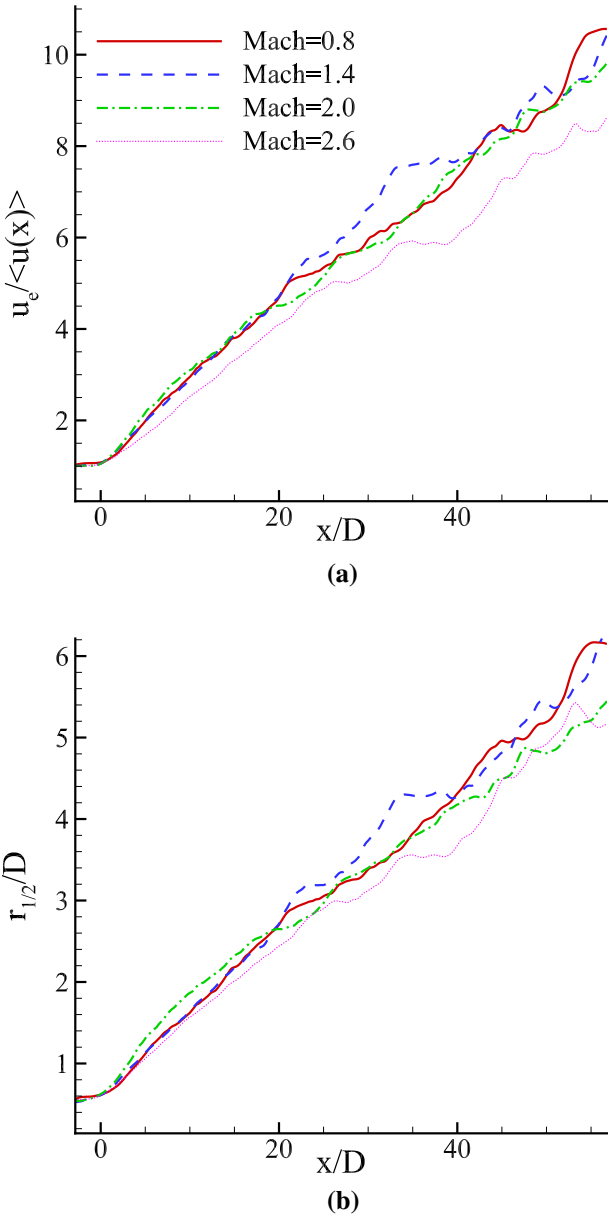

Fig. 9 **a** Inverse normalized centerline mean streamwise velocity and **b** normalized mean half-width vs normalized streamwise distance for different Mach numbers. Profiles are translated by the potential core length

which develops in the shear layer near the end of the potential core, is more quickly dissipated into internal energy (see also Fig. 16 and the discussion about the dissipation mechanism at the end of this section).

Figure 11a, b show the contour plots of the normalized $\overline{\overline{\text{TKE}}}$ for different Mach numbers and Re equal to 10,000 and different Reynolds numbers with Mach equal to 1.4,

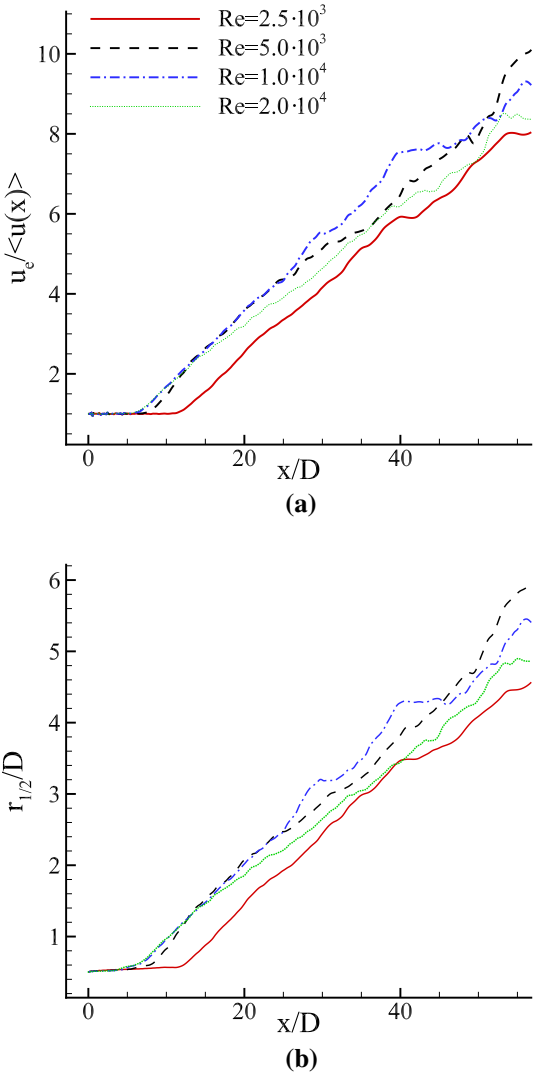

Fig. 10 **a** Inverse normalized centerline mean streamwise velocity and **b** normalized mean half-width vs normalized streamwise distance for different Reynolds numbers

respectively. Such figures show an increase of $\overline{\overline{\text{TKE}}}$ at a longer distance from the jet exit with an increase of the Mach number. This is due to a strong shear flow which generates and transports turbulence towards the jet centerline. Compressibility effects delay turbulence transition, which, on the other hand, is promoted by increasing Reynolds numbers.

Figure 12 shows the normalized $\overline{\overline{\text{TKE}}}$ (a) along the streamwise direction at the radial location where the $\overline{\overline{\text{TKE}}}$ peak value is reached, (b) the same profile as (a) but translated by the potential core length and (c) along the centerline as a function of the normalized streamwise distance for the gas jets with different Mach numbers. Figure 12a shows that compressibility effects delay turbulence transition since $\overline{\overline{\text{TKE}}}$ starts to grow further downstream by increasing the Mach number. The peak value of $\overline{\overline{\text{TKE}}}$ decreases by increasing Mach: a slow reduction of the peak value is observed with Mach number up to 2.0, whereas

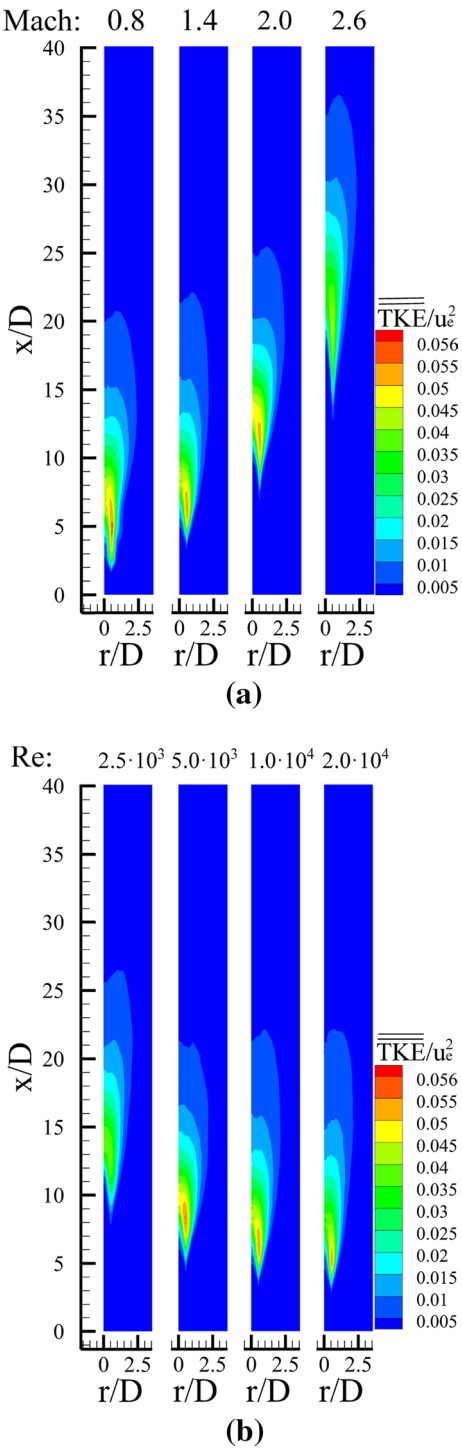

Fig. 11 Normalized $\overline{\overline{TKE}}$ contour plots: **a** Mach number effects; **b** Reynolds number effects

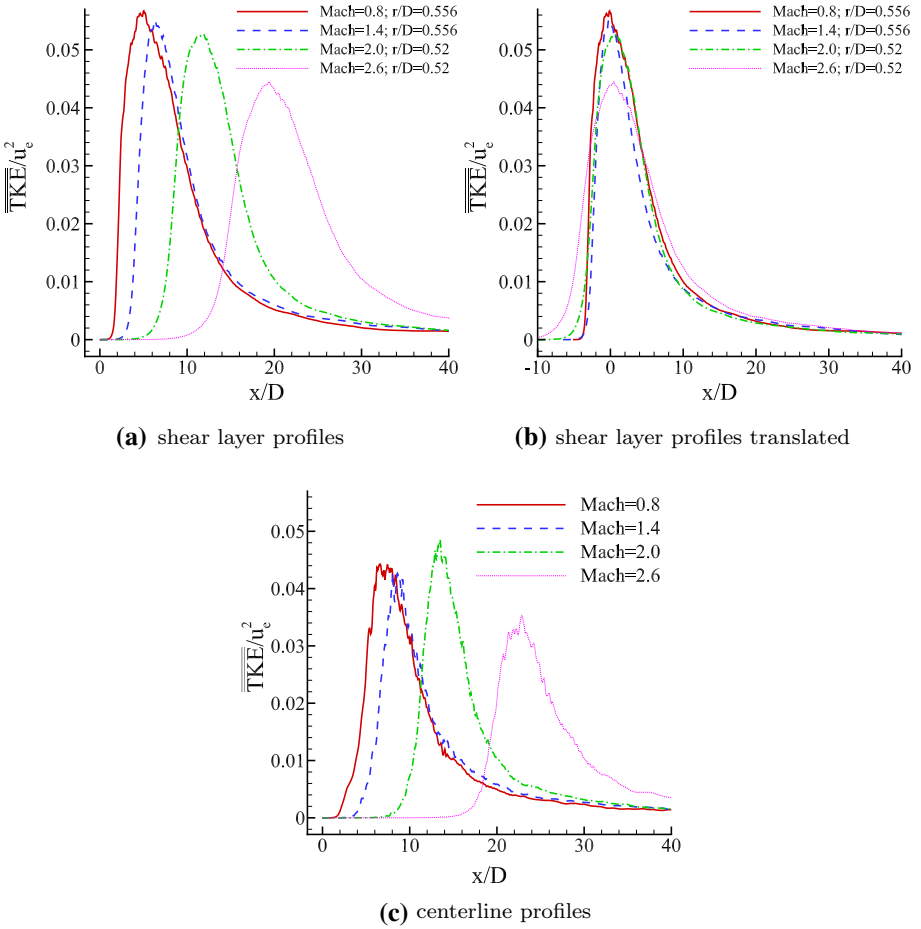

(a) shear layer profiles

(b) shear layer profiles translated

(c) centerline profiles

Fig. 12 Normalized $\overline{TKE}$ profiles for different Mach numbers: **a** along the streamwise direction at *r/D* where the peak value is reached (see legend and Fig. 11a); **b** the same profile as (**a**) but translated by the potential core length; **c** along the centerline

the peak value is considerably smaller for the case with $M = 2.6$. Moreover, the translated profiles of Fig. 12b show that, at some diameter downstream of the potential core, such profiles are almost on top of each other, to recover the same decay rate shown in Fig. 9a.

On the other hand Fig. 12c does not show a monotonic reduction of the $\overline{TKE}$ peak value with the Mach number even if an important reduction is observed at $M = 2.6$. Indeed, plotting each component of the turbulent intensities (see Fig. 13a–c), it can be seen that the peak value of the streamwise component does not show significant variations by changing the Mach number. On the other hand, the peak value of the spanwise components is nearly constant up to Mach number equal to 2.0 whereas it shows an important reduction at Mach number equal to 2.6. Therefore, along the centerline, compressibility affects only the spanwise turbulence intensities as the Mach number is larger than 2.0. A bit larger value of the $\overline{TKE}$ is observed along the centerline for $M = 2.0$ since at this Mach number turbulence is isotropic (see Fig. 14c and its discussion), whereas a strong anisotropy arises at $M = 2.6$

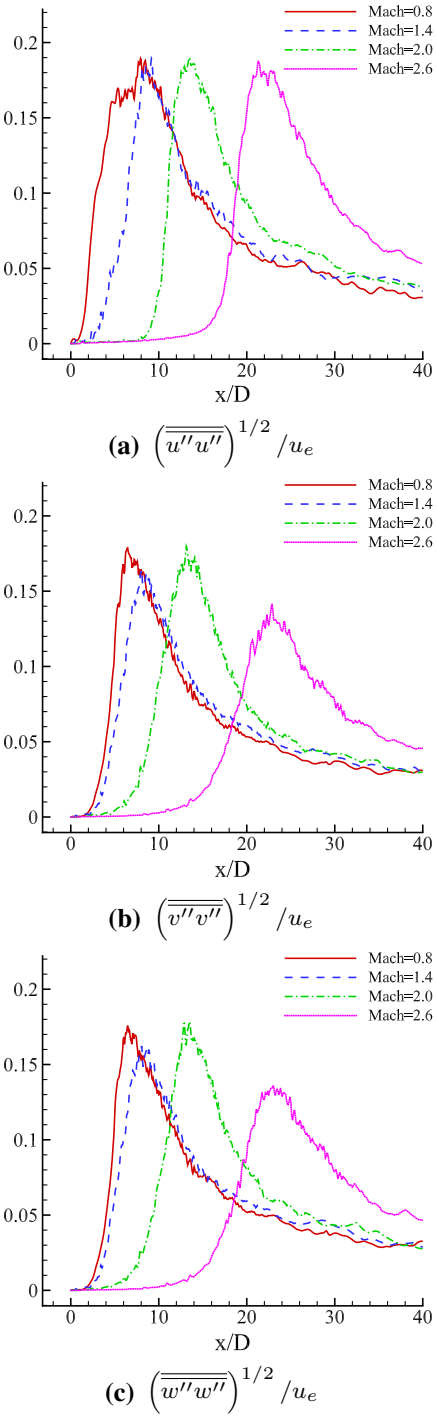

Fig. 13 Normalized turbulence intensities centerline profiles vs Mach number

(due to the reduction of the spanwise components). Likely, with this Mach number (2.6), the Re number is not sufficient to promote the growth of spanwise fluctuations and this behavior appears similar to that of Mach 1.4 at smaller Re (see Fig. 17a).

In order to gain more insights as regards TKE and strengthen previous discussion, Fig. 14 shows the centerline profiles of turbulence intensities normalized by the jet exit velocity for different Mach numbers. Compressibility seems to affect first the streamwise component of the gas velocity fluctuations and then the spanwise ones. Indeed, with Mach equal to 0.8 (Fig. 14a) the streamwise component grows earlier with respect to the other components. For the case with $M = 1.4$ (Fig. 14b), the streamwise component of gas velocity fluctuations begins to grow at the same location as the spanwise ones. Such spanwise components start to increase at roughly the same location of the $M = 0.8$ case. Moving from Mach 1.4 to Mach 2.0 (Fig. 14c), all components of the gas velocity fluctuations begin to grow later with respect to the cases with lower Mach number, with the streamwise component that starts to grow later than the spanwise ones. Finally, with Mach number equal to 2.6 (Fig. 14d), the delay of turbulence transition is more pronounced and

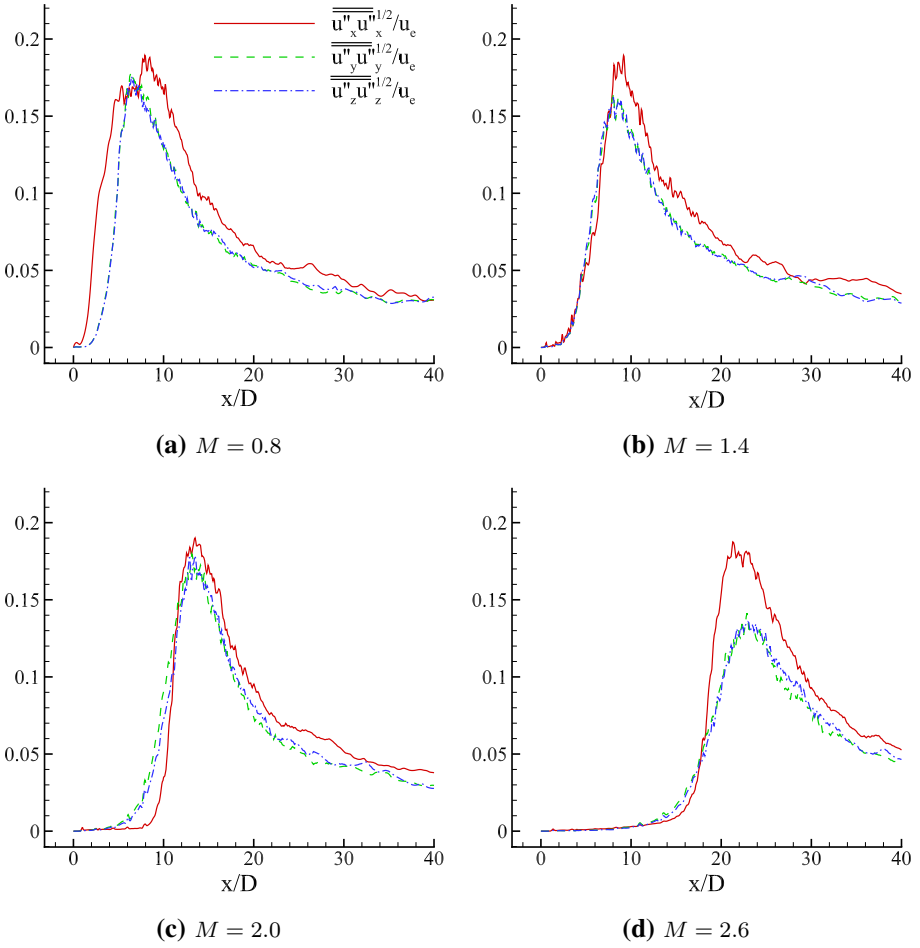

Fig. 14 Normalized turbulence intensities centerline profiles vs Mach number

a significant anisotropy arises. Indeed, in this case the spanwise components of the gas velocity fluctuations are considerably smaller than the streamwise component, and this is in contrast with the other cases where the three different components show almost the same peak values. Figure 15 shows the turbulence intensities for different Mach numbers along the streamwise direction at the radial location where the peak value of $\overline{\overline{\mathrm{TKE}}}$ is located. The figure shows that, by increasing Mach number, the turbulence transition occurs further downstream from the jet exit location and this is more evident for the spanwise components of the gas velocity fluctuations with respect to the streamwise component.

A similar $\overline{\overline{\mathrm{TKE}}}$ analysis has been performed with different Reynolds number for a given Mach number. Figure 16a shows the normalized $\overline{\overline{\mathrm{TKE}}}$ along the centerline as a function of the normalized streamwise distance for the gas jets with different Re. Turbulence transition is promoted by increasing Re, but for Re larger than 5000, the $\overline{\overline{\mathrm{TKE}}}$ peak value decreases with Re. Conversely, going from Re 2500 to 5000 the $\overline{\overline{\mathrm{TKE}}}$ peak value

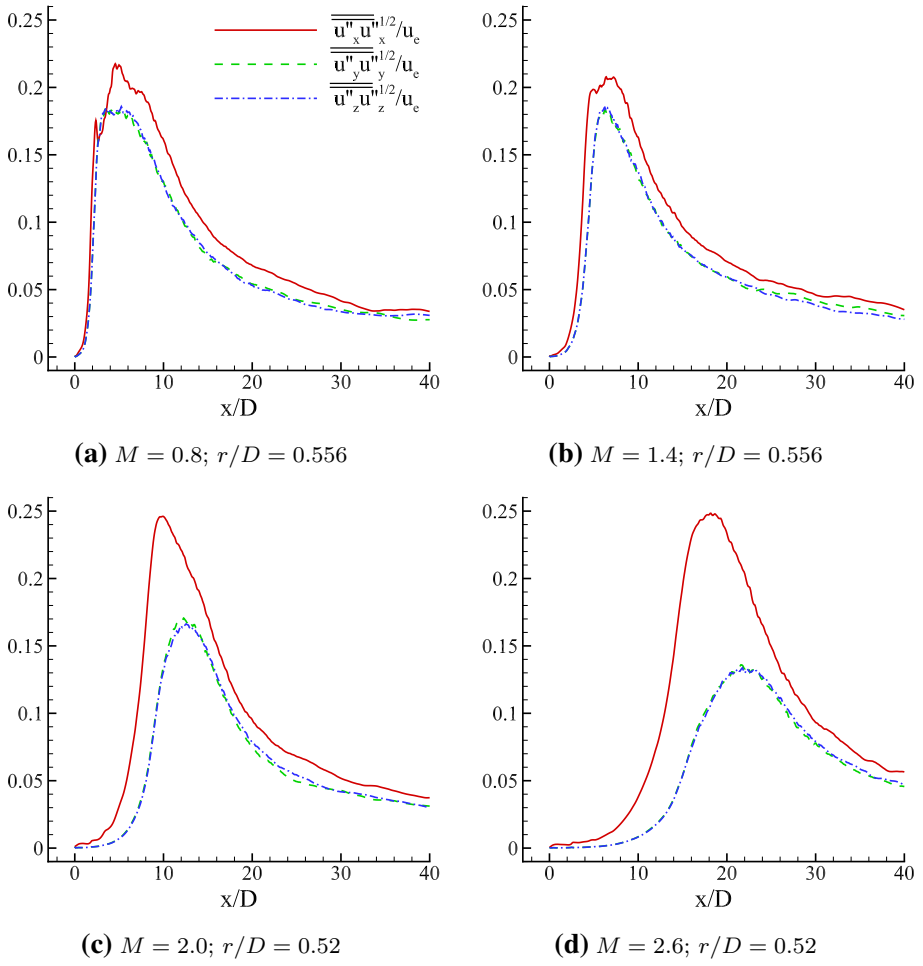

Fig. 15 Normalized turbulence intensities profiles along the streamwise direction vs Mach number at *r/D* where the peak value is located (see Fig. 11a)

increases. Indeed, for Re > 5000 a fully turbulent condition is recovered, thus finer turbulent length scales are present and TKE is dissipated faster into internal energy (see also the discussion about dissipation mechanism given at the end of this section). Moreover, by increasing Re, the peak value of $\overline{\overline{\mathrm{TKE}}}$ occurs in the shear layer at larger radial distance from the centerline, as shown in Fig. 16b. In the figure, the normalized $\overline{\overline{\mathrm{TKE}}}$ as

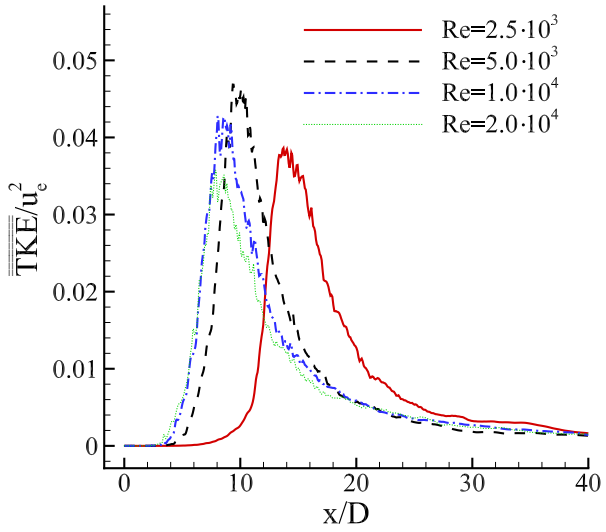

(a) centerline profiles

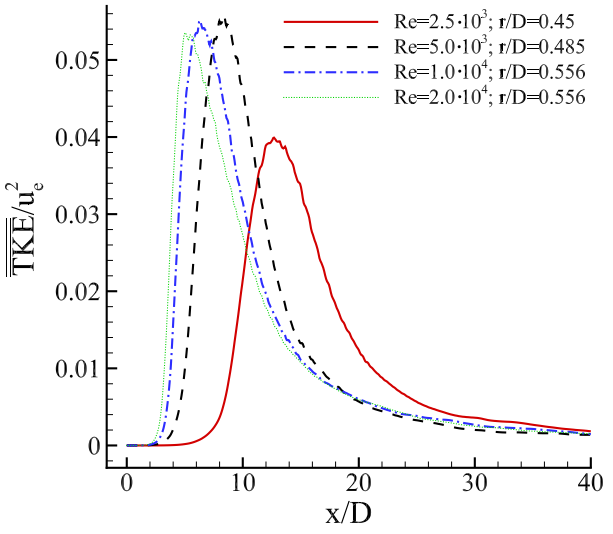

(b) shear layer profiles

Fig. 16 Normalized $\overline{\overline{\mathrm{TKE}}}$ profiles for different Reynolds numbers: **a** along the centerline; **b** along the streamwise direction at *r/D* where the peak value is located (see legend and Fig. 11b)

a function of x/D at the radial location where the peak value occurs is given. The radial distance where the peak of $\overline{\overline{\mathrm{TKE}}}$ is located tends to a constant value for Re higher than 10,000. The peak value of $\overline{\overline{\mathrm{TKE}}}$ is lower for $Re = 2500$, whereas for the other cases similar peak values are obtained.

Figures 17 and 18 show the turbulence intensities centerline profiles and streamwise profiles at the radial location where the peak value of $\overline{\overline{\mathrm{TKE}}}$ occurs for different Reynolds numbers, respectively. Once more, it is noticed that turbulence transition starts earlier by increasing Re. Moreover, similar to the case with $M = 2.6$ and $Re = 10{,}000$ (Fig. 14d), a strong anisotropic behavior is observed with $M = 1.4$ and $Re = 2500$ (Fig. 17a). This anisotropy tends to disappear by increasing Re.

In order to better understand the mechanism behind turbulence production and dissipation, all terms of the $\overline{\overline{\mathrm{TKE}}}$ equations have been analysed. The steady state Favre-averaged turbulence kinetic energy equation (Wilcox 1994; Bogey and Bailly 2006) reads:

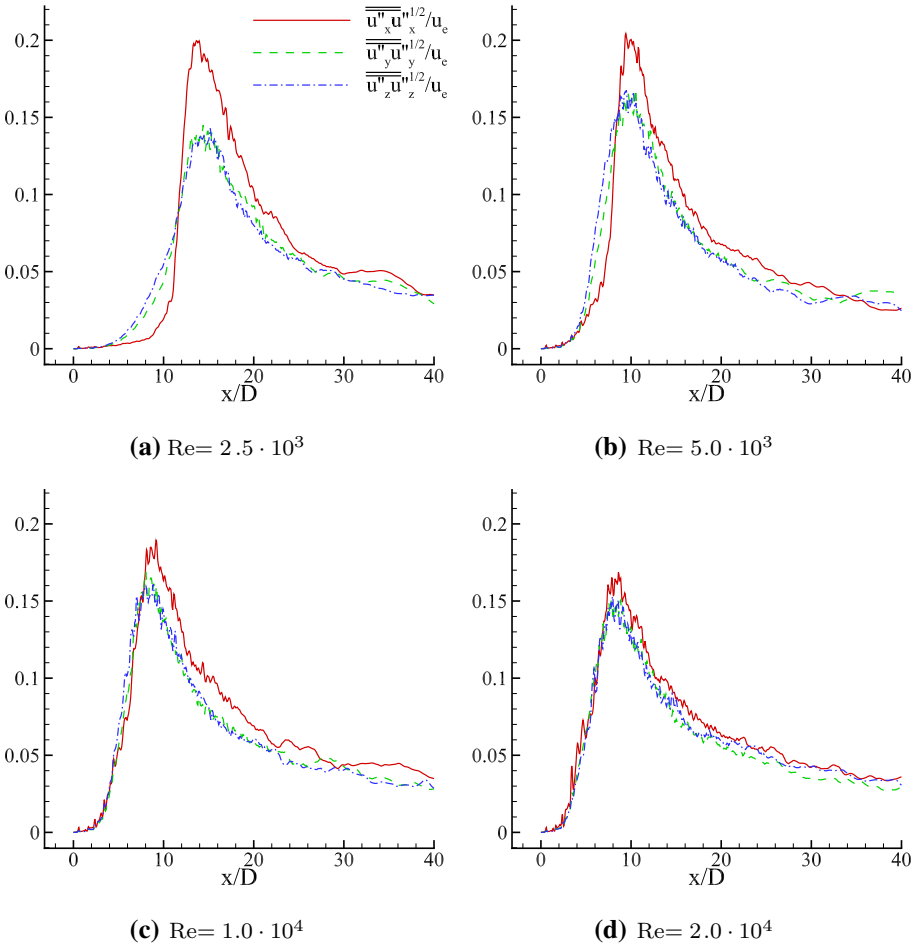

Fig. 17 Normalized turbulence intensities centerline profiles vs Reynolds number

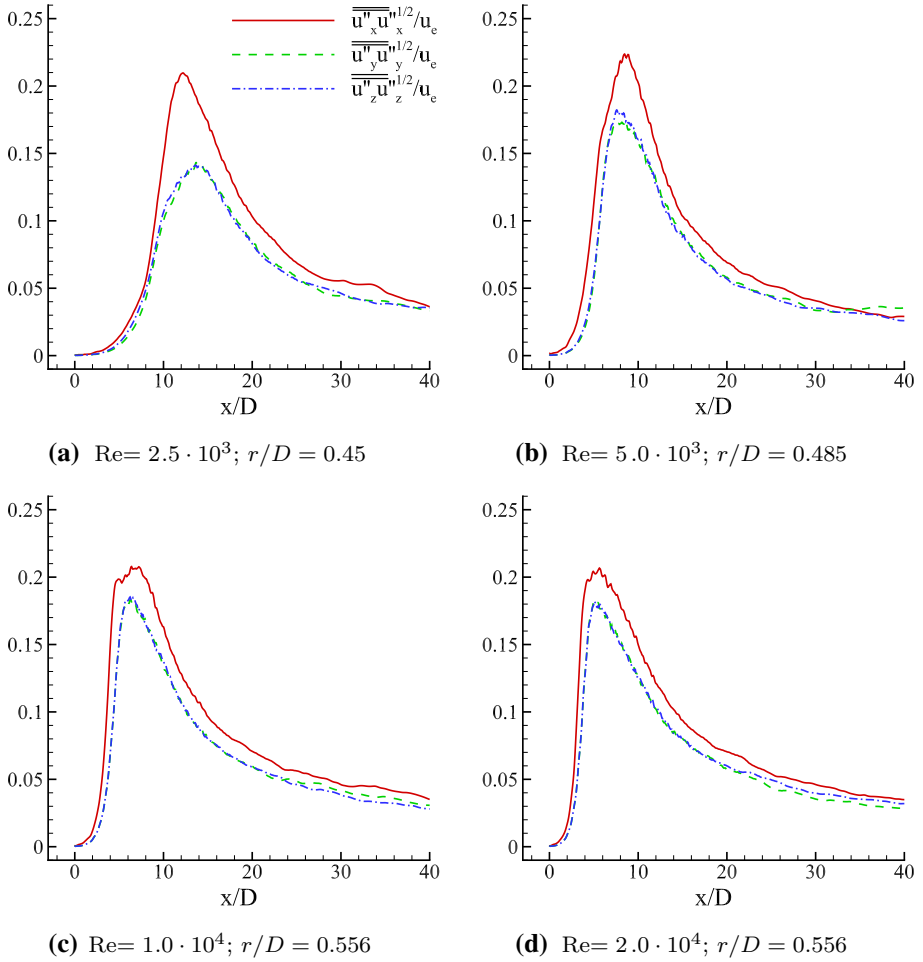

(a) Re$= 2.5 \cdot 10^3$; $r/D = 0.45$ **(b)** Re$= 5.0 \cdot 10^3$; $r/D = 0.485$

(c) Re$= 1.0 \cdot 10^4$; $r/D = 0.556$ **(d)** Re$= 2.0 \cdot 10^4$; $r/D = 0.556$

Fig. 18 Normalized turbulence intensities profiles along the streamwise direction vs Reynolds number at *r/D* where the peak value is located (see Fig. 11a)

$$\underbrace{\langle\rho\rangle\,\tilde{\bar{u}}_j\frac{\partial\overline{\overline{TKE}}}{\partial x_j}}_{\text{convection}} - D_{filter} = \underbrace{\tau_{i,j}\frac{\partial\tilde{\bar{u}}_i}{\partial x_j}}_{\text{production}} - \underbrace{\left\langle t_{j,i}\frac{\partial u''_i}{\partial x_j}\right\rangle}_{\text{viscous dissipation}} + \underbrace{\frac{\partial\left\langle t_{j,i}u''_i\right\rangle}{\partial x_j}}_{\text{molecular diffusion}}$$
$$\underbrace{-\frac{\partial\left\langle\rho u''_j\frac{1}{2}u''_i u''_i\right\rangle}{\partial x_j}}_{\text{turbulence diffusion}} \underbrace{-\frac{\partial\left\langle p'u''_j\right\rangle}{\partial x_j}}_{\text{pressure diffusion}} \underbrace{-\left\langle u''_i\right\rangle\frac{\partial\langle p\rangle}{\partial x_i}}_{\text{pressure work}} + \underbrace{\left\langle p'\frac{\partial u''_i}{\partial x_i}\right\rangle}_{\text{pressure dilatation}}. \tag{9}$$

In the above equation p is the pressure, $\tau_{i,j}$ and $t_{i,j}$ are the Favre-averaged Reynolds-stress tensor and the viscous stress tensor, respectively, i.e.:

$$\tau_{i,j} = -\left\langle \rho u_i'' u_j'' \right\rangle \tag{10}$$

$$t_{i,j} = \mu\left(\frac{\partial u_i}{\partial x_j} + \frac{\partial u_j}{\partial x_i}\right) - \frac{2}{3}\mu\frac{\partial u_k}{\partial x_k}\delta_{i,j}, \tag{11}$$

where μ is the dynamic viscosity. D_{filter} is the dissipation term due to smallest turbulent scales that, following the work of Bogey and Bailly (2006), has been evaluated as the balance of the remaining terms.

With respect to the TKE equation of an incompressible fluid, Eq. (9) has two additional terms, i.e., the pressure-work and the pressure-dilatation terms. As expected, both terms vanish in the limit of incompressible fluid (Wilcox 1994). One could expect that the differences in the jet mixing properties at increasing Mach numbers are mainly due to such terms. However, from Fig. 19, where each term of Eq. (9) is shown for Mach 1.4 and 2.6 and Re equal to 1.0×10^4, it follows that pressure work and pressure dilatation contributions are negligible even at the largest Mach number. Indeed, the modification of the jet structure, as Mach number increases, is mainly due to the production term. Such contribution is important at smaller Mach numbers, thus causing a larger TKE in the shear layer as shown in Fig. 12a. Moreover, turbulence diffusion and pressure diffusion contributions decrease as Mach number increases, and this explains the lower spanwise turbulence intensities for the larger Mach numbers shown in Fig. 15.

Further details of the turbulent kinetic energy budget for all Mach numbers is provided in Fig. 20. The right hand side of Eq. (9) (Fig. 20a) shows that the smaller is the Mach number the larger is the TKE convection and, as previously stated, this confirms the importance of the production term, as shown in Fig. 20b.

As regards the dissipation mechanism, it is worth noting that both viscous and filter dissipation contributions decrease as Mach number increases (Fig. 20c, d). Filtering

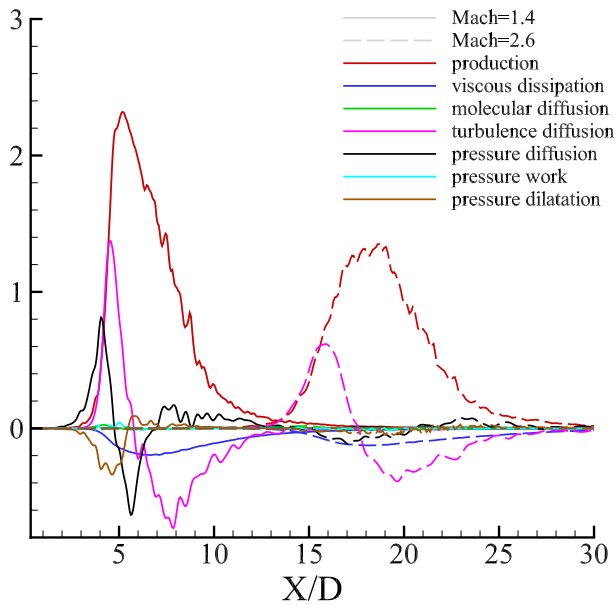

Fig. 19 Normalized (by $\rho_e u_e^3$) kinetic energy budget [1/m] along the streamwise direction at $r/D = 0.42$, where the right hand side of Eq. (9) is maximum, for Mach number equal to 1.4 and 2.6

dissipation appears to be larger than the viscous one for all cases and its relative contribution to the total dissipation (viscous plus filter) remains the same.

Finally, the main differences of the TKE budget, related to the Mach number, are concentrated in the region near the end of the potential core where larger gradients are located. This explains why compressibility effects are negligible downstream of the potential core (Figs. 9 and 12b).

The same analysis has been performed for the Reynolds number. Fig. 21 shows the contributions of Eq. (9) for Re equal to 2.5×10^3 and 2.0×10^4 with a Mach number equal to 1.4. The change of the TKE budget as Re increases is opposite with respect to the Mach number increase. The higher is the Reynolds number, the higher are the production, the turbulence and the pressure diffusion terms. Therefore, the production term promotes a local TKE gain and a TKE diffusion occurs due to the corresponding contributions. This mechanism explains the trends shown in Fig. 16b, where a similar peak value of TKE has

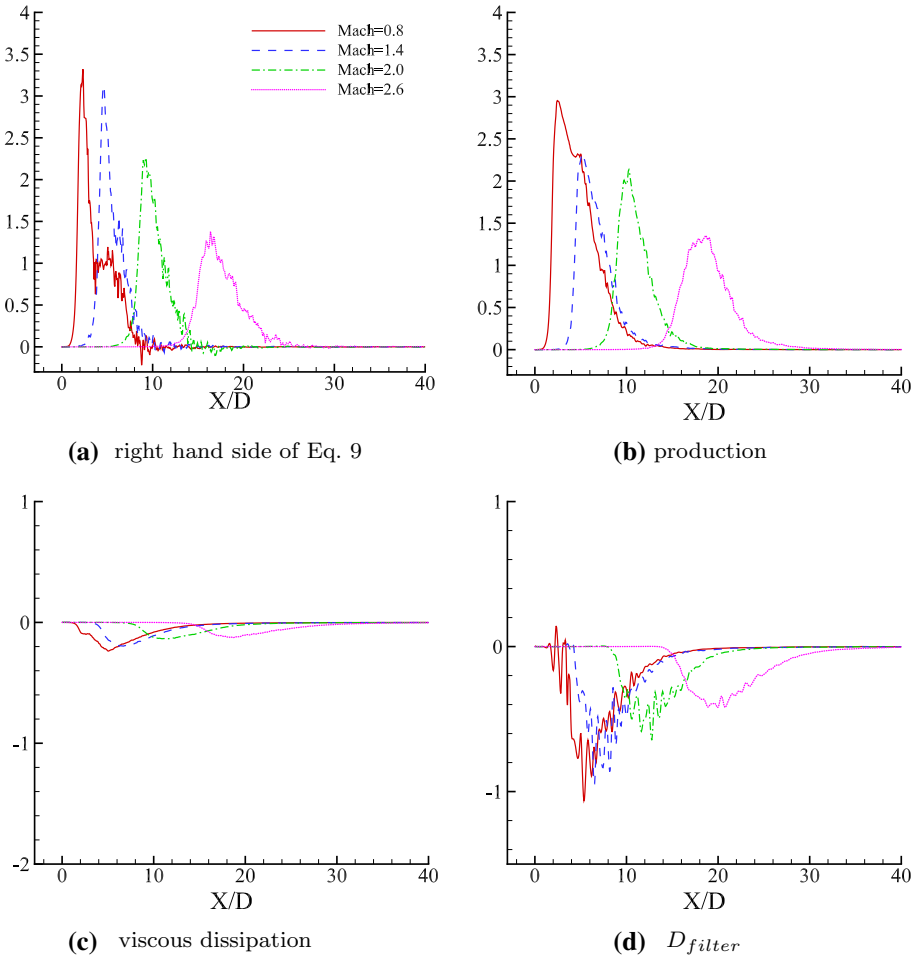

(a) right hand side of Eq. 9 **(b)** production

(c) viscous dissipation **(d)** D_{filter}

Fig. 20 Normalized (by $\rho_e u_e^3$) kinetic energy budget [1/m] along the streamwise direction vs Mach number at $r/D = 0.42$, where the right hand side of Eq. (9) is maximum: **a** right hand side of Eq. (9); **b** production; **c** viscous dissipation; **d** filtering dissipation

been found for all cases with Re higher than 5000. Indeed, at such Reynolds numbers, the production and the diffusion terms balance and an almost isotropic behavior is observed for the turbulence intensities, as shown in Figs. 17 and 18. For Re equal to 2500, a lower production term causes a lower TKE (Fig. 16). Diffusion terms are negligible and a non-isotropic behavior of turbulence intensities (Figs. 17a and 18a) is observed. Other details are given in Fig. 22a, b to confirm such an analysis, where the right hand side of Eq. (9) and the production term are given for all the investigated Reynolds numbers.

As regards the influence of Re on the dissipation mechanism, Fig. 22c, d show that, as Re increases, viscous dissipation decreases whereas filtering dissipation increases. This has already been discussed by Bogey and Bailly (2006). Indeed, finer turbulent eddies are present and they need to be modelled as Re increases (see also Fig. 5). Hence, the D_{filter} contribution becomes more important and, at large Re, TKE is dissipated faster into internal energy. This confirms the smaller values of TKE along the jet centerline (Fig. 16a) and the smaller velocity decay and spreading rate (Fig. 10).

5 Conclusions

Mach and Reynolds numbers effects on the behaviour of turbulent round jets have been examined by employing an in-house LES solver. Such approach has allowed to untangle the question of whether compressibility has relevant effects on velocity decay rate and spreading rate. This question is important to improve turbulence closure models widely used in commercial codes to design applications in the field of aerospace propulsion and in the automotive sector.

This work considerably improves the few numerical and experimental works that addressed the same topic. Indeed previous works may not give a satisfactory description of what occurs downstream of the potential core. Both Maidi and Lesieur (2005) and Bellan (2016) employ a relatively small computational domain ($25D \times 8D \times 8D$ (Bellan

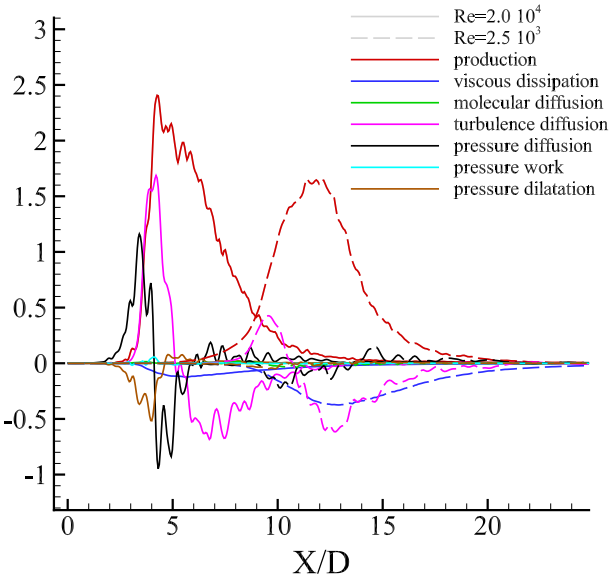

Fig. 21 Normalized (by $\rho_e u_e^3$) kinetic energy budget [1/m] along the streamwise direction at $r/D = 0.42$, where the right hand side of Eq. (9)is maximum for Reynolds numbers equal to 2.5×10^3 and 2.0×10^4

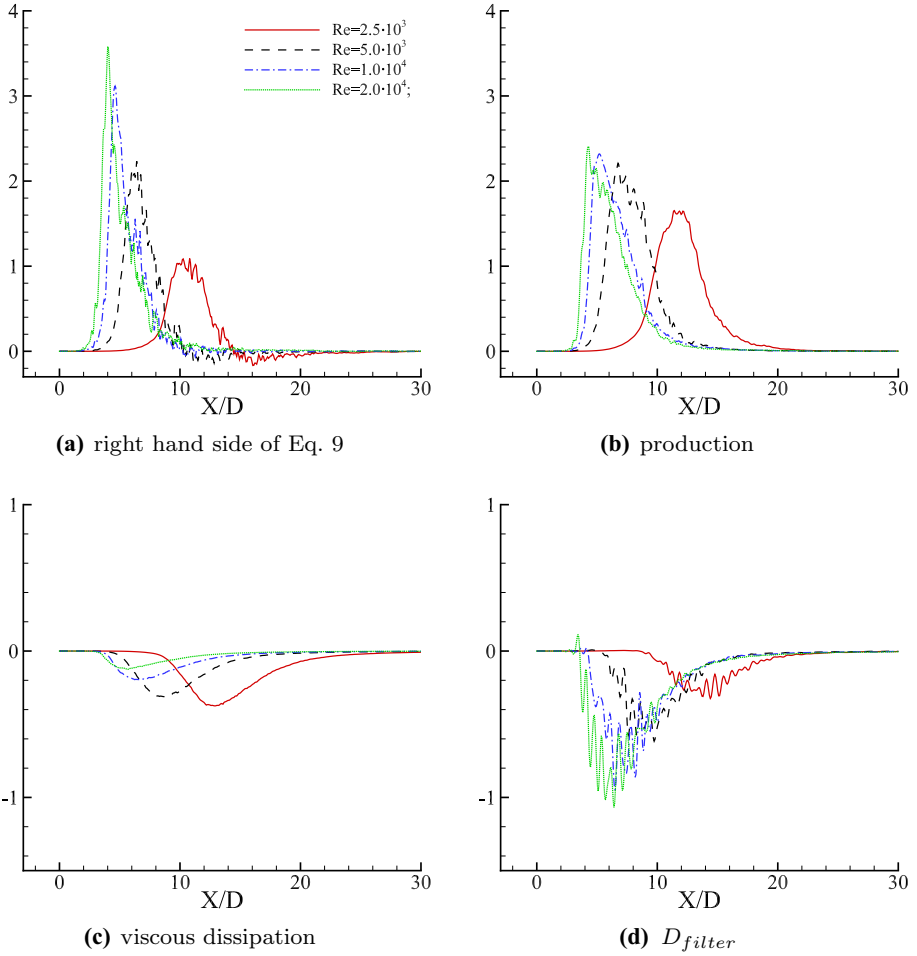

Fig. 22 Normalized (by $\rho_e u_e^3$) kinetic energy budget [1/m] along the streamwise direction vs Reynolds number at $r/D = 0.42$, where the right hand side of Eq. (9) is maximum: **a** right hand side of Eq. (9); **b** production; **c** viscous dissipation; **d** filtering dissipation

2016), $17.5D \times 10D \times 10D$ (Maidi and Lesieur 2005)) and a definite statement on compressibility effects in the far field region cannot be given. Furthermore, this is the first numerical work where the compressibility effect is isolated from other effects by changing only the exit Mach number while retaining the same exit jet momentum and the same Reynolds number. Furthermore, with respect to previous works a wider range of Mach from 0.8 to 2.6 is investigated.

Mach numbers from 0.8 to 2.6 with Re equal to 10,000 have been considered. The results of the simulations show that compressibility strongly affects the potential core length but it does not affect the velocity decay and spreading rates downstream of the potential core up to M = 2.0, whereas in the case with Mach equal to 2.6 the velocity decay and spreading rates decrease. An analysis of the streamwise and spanwise

components of turbulence intensities shows that a significant anisotropy for the case with Mach number equal to 2.6 occurs.

The influence of Reynolds number on the gas jet has been explored in the range 2500–20,000 by keeping Mach number equal to 1.4. The results show that the potential core length decreases by increasing Re up to 10,000. For higher Reynolds numbers, the potential core length does not change significantly. The velocity decay rate and the spreading rate are slower by increasing Re from 10,000 to 20,000, whereas no influences are appreciated for Re up to 10,000.

Acknowledgements We acknowledge the CINECA Awards N.HP10BUD7FQ, under the ISCRA initiative, for the availability of high performance computing resources and support. This work was partially supported by the Italian Ministry of Education, University and Research under the Programme Department of Excellence Legge 232/2016 (Grant No. CUP - D94I18000260001).

Funding Open Access funding provided by Politecnico di Bari.

Compliance with ethical standards

Conflict of Interest The authors declare that they have no conflict of interest.

References

Abraham, J., Magi, V.: Exploring velocity ratio and density ratio effects in a mixing layer using DNS. Int. J. Comput. Fluid Dyn. **8**(2), 147–151 (1997). https://doi.org/10.1080/10618569708940801

Amielh, M., Djeridane, T., Anselmet, F., Fulachier, L.: Velocity near-field of variable density turbulent jets. Int. J. Heat Mass Transf. **39**(10), 2149–2164 (1996). https://doi.org/10.1016/0017-9310(95)00294-4

Anders, J.W.: Turbulence and residual gas effects in pulsed diesel jets. PhD Thesis, School of Mechanical Engineering, Purdue University, West Lafayette, Indiana (2006)

Anders, J.W., Magi, V., Abraham, J.: Large-eddy simulation in the near-field of a transient multi-component gas jet with density gradients. Comput. Fluids **36**(10), 1609–1620 (2007). https://doi.org/10.1016/j.compfluid.2007.03.002

Ball, C.G., Fellouah, H., Pollard, A.: The flow field in turbulent round free jets. Prog. Aerosp. Sci. **50**, 1–26 (2012). https://doi.org/10.1016/j.paerosci.2011.10.002

Bellan, J.: Large-eddy simulation of supersonic round jets: effects of Reynolds and Mach numbers. AIAA J. **54**(5), 1482–1498 (2016). https://doi.org/10.2514/1.J054548

Boersma, B.J., Lele, S.K.: Large eddy simulation of compressible turbulent jets. Cent. Turbul. Res. Annu. Res. Briefs (1999)

Bogey, C., Bailly, C.: Large eddy simulations of transitional round jets: influence of the Reynolds number on flow development and energy dissipation. Phys. Fluids **18**(6), 065101 (2006). https://doi.org/10.1063/1.2204060

Bogey, C., Bailly, C., Juvé, D.: Noise investigation of a high subsonic, moderate Reynolds number jet using a compressible large eddy simulation. Theoret. Comput. Fluid Dyn. **16**(4), 273–297 (2003). https://doi.org/10.1007/s00162-002-0079-4

Boguslawski, L., Popiel, C.O.: Flow structure of the free round turbulent jet in the initial region. J. Fluid Mech. **90**(3), 531–539 (1979). https://doi.org/10.1017/S0022112079002378

Bonelli, F.: A numerical investigation of turbulent compressible hydrogen jets. PhD Thesis, School of Engineering, University of Basilicata, Potenza, Italy (2013)
Bonelli, F., Viggiano, A., Magi, V.: A numerical analysis of hydrogen underexpanded jets. In: Proceedings of the ASME 2012 Internal Combustion Engine Division Spring Technical Conference, ICES2012. ASME, pp. 681–690 (2012). https://doi.org/10.1115/ICES2012-81068
Bonelli, F., Viggiano, A., Magi, V.: Large eddy simulation of high-density ratio hydrogen jet. In: 11th International Conference of Numerical Analysis and Applied Mathematics (ICNAAM 2013), AIP Conference Proceedings, vol. 1558, pp. 232–235 (2013a). https://doi.org/10.1063/1.4825463
Bonelli, F., Viggiano, A., Magi, V.: A numerical analysis of hydrogen underexpanded jets under real gas assumption. J. Fluids Eng. **135**(12), 121101 1–121101 11 (2013b). https://doi.org/10.1115/1.4025253
Bonelli, F., Viggiano, A., Magi, V.: How does a high density ratio affect the near- and intermediate-field of high-re hydrogen jets? Int. J. Hydrog. Energy **41**(33), 15007–15025 (2016). https://doi.org/10.1016/j.ijhydene.2016.06.174
Bradshaw, P.: Compressible turbulent shear layers. Annu. Rev. Fluid Mech. **9**(1), 33–52 (1977). https://doi.org/10.1146/annurev.fl.09.010177.000341
Brès, G.A., Ham, F.E., Nichols, J.W., Lele, S.K.: Unstructured large-eddy simulations of supersonic jets. AIAA J. **55**(4), 1164–1184 (2017). https://doi.org/10.2514/1.J055084
Buchta, D.A., Freund, J.B.: The near-field pressure radiated by planar high-speed free-shear-flow turbulence. J. Fluid Mech. **832**, 383–408 (2017). https://doi.org/10.1017/jfm.2017.671
Chen, C., Rodi, W.: Vertical Turbulent Buoyant Jets: A Review of Experimental Data. Pergamon Press, Great Britain (1980)
Cook, A.W.: Artificial fluid properties for large-eddy simulation of compressible turbulent mixing. Phys. Fluids **19**, 055103 (2007). https://doi.org/10.1063/1.2728937
DeBonis, J.R., Scott, J.N.: Large-eddy simulation of a turbulent compressible round jet. AIAA J. **40**(7), 1346–1354 (2002). https://doi.org/10.2514/2.1794
Fellouah, H., Pollard, A.: The velocity spectra and turbulence length scale distributions in the near to intermediate regions of a round free turbulent jet. Phys. Fluids **21**(11), 115101 (2009). https://doi.org/10.1063/1.3258837
Fellouah, H., Ball, C.G., Pollard, A.: Reynolds number effects within the development region of a turbulent round free jet. Int. J. Heat Mass Transf. **52**(17–18), 3943–3954 (2009). https://doi.org/10.1016/j.ijheatmasstransfer.2009.03.029
Freund, J.B.: Noise sources in a low-Reynolds-number turbulent jet at Mach 0.9. J. Fluid Mech. **438**, 277–305 (2001). https://doi.org/10.1017/S0022112001004414
Freund, J.B.: Nozzles, turbulence, and jet noise prediction. J. Fluid Mech. **860**, 1–4 (2019). https://doi.org/10.1017/jfm.2018.823
Gill, S.: Process for the step-by-step integration of differential equations in an automatic computing machine. Proc. Camb. Philos. Soc. **47**, 96–108 (1951)
Gojon, R., Bogey, C., Mihaescu, M.: Large eddy simulation of highly compressible jets with tripped boundary layers. In: Salvetti, M.V., Armenio, V., Fröhlich, J., Geurts, B.J., Kuerten, H. (eds.) Direct and Large-Eddy Simulation XI, pp. 333–339. Springer, Cham (2019)
Gutmark, E.J., Schadow, K.C., Yu, K.H.: Mixing enhancement in supersonic free shear flows. Annu. Rev. Fluid Mech. **27**(1), 375–417 (1995). https://doi.org/10.1146/annurev.fl.27.010195.002111
Hamzehloo, A., Aleiferis, P.: Gas dynamics and flow characteristics of highly turbulent under-expanded hydrogen and methane jets under various nozzle pressure ratios and ambient pressures. Int. J. Hydrog. Energy **41**(15), 6544–6566 (2016). https://doi.org/10.1016/j.ijhydene.2016.02.017
Heisenberg, W.: On the theory of statistical and isotropic turbulence. Proc. R. Soc. A **195**, 402–406 (1948). https://doi.org/10.1098/rspa.1948.0127
Hirsch, C.: Numerical Computation of Internal and External Flows: Volume 1 Fundamentals of Computational Fluid Dynamics, 2nd edn. Butterworth–Heinemann, Linacre House, Jordan Hill, Oxford OX2 8DP, 30 Corporate Drive, Suite 400, Burlington, MA 01803, USA (2007)
Hussein, H.J., Capp, S.P., George, W.K.: Velocity measurements in a high-Reynolds-number, momentum-conserving, axisymmetric, turbulent jet. J. Fluid Mech. **258**, 31–75 (1994). https://doi.org/10.1017/S002211209400323X
Jordan, P., Colonius, T.: Wave packets and turbulent jet noise. Annu. Rev. Fluid Mech. **45**(1), 173–195 (2013). https://doi.org/10.1146/annurev-fluid-011212-140756
Kawai, S., Lele, S.K.: Localized artificial diffusivity scheme for discontinuity capturing on curvilinear meshes. J. Comput. Phys. **227**(22), 9498–9526 (2008). https://doi.org/10.1016/j.jcp.2008.06.034
Lau, J.C.: Effects of exit Mach number and temperature on mean-flow and turbulence characteristics in round jets. J. Fluid Mech. **105**, 193–218 (1981). https://doi.org/10.1017/S0022112081003170

Lau, J.C., Morris, P.J., Fisher, M.J.: Measurements in subsonic and supersonic free jets using a laser velocimeter. J. Fluid Mech. **93**(1), 1–27 (1979). https://doi.org/10.1017/S0022112079001750
Lele, S.K.: Compact finite difference schemes with spectral-like resolution. J. Comput. Phys. **103**(1), 16–42 (1992). https://doi.org/10.1016/0021-9991(92)90324-R
Lele, S.K.: Compressibility effects on turbulence. Annu. Rev. Fluid Mech. **26**(1), 211–254 (1994). https://doi.org/10.1146/annurev.fl.26.010194.001235
Li, D., Fan, J., Cen, K.: Direct numerical simulation of the entrainment coefficient and turbulence properties for compressible spatially evolving axisymmetric jets. Fuel **102**, 470–477 (2012). https://doi.org/10.1016/j.fuel.2012.01.029. special Section: ACS Clean Coal
Maidi, M., Lesieur, M.: Large eddy simulations of spatially growing subsonic and supersonic turbulent round jets. J. Turbul. **6**, N38 (2005). https://doi.org/10.1080/14685240500125518
Morkovin M (1962) Effects of compressibility on turbulent flow. In: The Mechanics of Turbulence ed. A Favre, Gordon and Breach, pp. 367–80
Morrison, G.L., McLaughlin, D.K.: Instability process in low Reynolds number supersonic jets. AIAA J. **18**(7), 793–800 (1980). https://doi.org/10.2514/3.7688
Panchapakesan, N.R., Lumley, J.L.: Turbulence measurements in axisymmetric jets of air and helium. Part 1. air jet. J. Fluid Mech. **246**, 197–223 (1993). https://doi.org/10.1017/S0022112093000096
Papamoschou, D., Roshko, A.: The compressible turbulent shear layer: an experimental study. J. Fluid Mech. **197**, 453–477 (1988). https://doi.org/10.1017/S0022112088003325
Poinsot, T.J., Lele, S.K.: Boundary conditions for direct simulations of compressible viscous flows. J. Comput. Phys. **101**(1), 104–129 (1992). https://doi.org/10.1016/0021-9991(92)90046-2
Pope, S.B.: Turbulent Flows. Cambridge University Press, Cambridge (2000)
Pope, S.B.: Ten questions concerning the large-eddy simulation of turbulent flows. New J. Phys. **6**, 35 (2004). https://doi.org/10.1088/1367-2630/6/1/035
Sautet, J.C., Stepowski, D.: Dynamic behavior of variable-density, turbulent jets in their near development fields. Phys. Fluids **7**(11), 2796–2806 (1995). https://doi.org/10.1063/1.868658
Sayeed, M., Magi, V., Abraham, J.: Enhancing the performance of a parallel solver for turbulent reacting flow simulations. Numer. Heat Transf. Part B Fundam. **59**(3), 169–189 (2011). https://doi.org/10.1080/10407790.2011.550527
Tam, C.K.W.: Supersonic jet noise. Annu. Rev. Fluid Mech. **27**(1), 17–43 (1995). https://doi.org/10.1146/annurev.fl.27.010195.000313
Wang, P., Frohlich, J., Michelassi, V., Rodi, W.: Large-eddy simulation of variable-density turbulent axisymmetric jets. Int. J. Heat Fluid Flow **29**(3), 654–664 (2008). https://doi.org/10.1016/j.ijheatfluidflow.2008.02.002
Wang, Z., Andreopoulos, Y.: Density and compressibility effects in turbulent subsonic jets part 1: mean velocity field. Exp. Fluids **48**(2), 327–343 (2010). https://doi.org/10.1007/s00348-009-0738-y
Weisgraber, T.H., Liepmann, D.: Turbulent structure during transition to self-similarity in a round jet. Exp. Fluids **24**(3), 210–224 (1998). https://doi.org/10.1007/s003480050168
Welch, P.D.: The use of fast Fourier transform for the estimation of power spectra: a method based on time averaging over short, modified periodograms. Audio Electroacoustics IEEE Trans. **15**(2), 70–73 (1967). https://doi.org/10.1109/TAU.1967.1161901
Wilcox, D.C.: Turbulence Modeling for CFD. DCW Industries Inc., La Cañada (1994)
Witze, P.: Centerline velocity decay of compressible free jets. AIAA J. **12**(4), 417–418 (1974). https://doi.org/10.2514/3.49262
Wygnanski, I., Fiedler, H.: Some measurements in the self-preserving jet. J. Fluid Mech. **38**(3), 577–612 (1969). https://doi.org/10.1017/S0022112069000358
Xu, G., Antonia, R.: Effect of different initial conditions on a turbulent round free jet. Exp. Fluids **33**(5), 677–683 (2002). https://doi.org/10.1007/s00348-002-0523-7
Zaman, K.B.M.Q.: Far-field noise of a subsonic jet under controlled excitation. J. Fluid Mech. **152**, 83–111 (1985). https://doi.org/10.1017/S0022112085000581
Zaman, K.B.M.Q.: Asymptotic spreading rate of initially compressible jets-experiment and analysis. Phys. Fluids **10**(10), 2652–2660 (1998). https://doi.org/10.1063/1.869778
Zaman, K.B.M.Q.: Spreading characteristics of compressible jets from nozzles of various geometries. J. Fluid Mech. **383**, 197–228 (1999). https://doi.org/10.1017/S0022112099003833